Green Chemistry

PAPER

View Article Online
View Journal | View Issue

Check for updates

Cite this: *Green Chem.*, 2026, **28**, 6241

Eco-efficient hydrolysis of coconut oil: a continuous hydrothermal and water-only process for the production of oleochemicals

Enkeledo Menalla,[a] Diego Martin,[a] Luis Vaquerizo,[a] Jefferson W. Tester,[b] María José Cocero[a] and Danilo Cantero *[a]

Received 2nd February 2026,
Accepted 27th February 2026

DOI: 10.1039/d6gc00718j

rsc.li/greenchem

A continuous hydrothermal process using water as reaction medium was investigated for the selective hydrolysis of triglycerides under sub- and supercritical conditions. The process was operated in continuous flow at 250–400 °C and 22–25 MPa with residence times between <1 s and <60 s, enabling controlled partial or near-complete hydrolysis without added catalysts, organic solvents and expensive enzymes. At 380 °C and 25 MPa, selective partial hydrolysis yielded up to 51 wt% mono-diglycerides and 32 wt% fatty acids at a residence time of 23 s. The process was demonstrated at a pilot scale with a throughput of 30 kg h^{-1} and stable operation at high oil concentrations up to 34 wt% in the reactor. Integration of counter-current heat recovery reduced the external energy demand by up to 61%, addressing the high energy intensity typically associated with supercritical water processing. Hydrolysates enriched in mono- and diglycerides exhibited strong emulsifying performance and long-term stability up to 1 year, comparable to that of a commercial emulsifier. These results show that continuous, water-only hydrothermal hydrolysis enables rapid and selective triglyceride conversion within an energy-integrated and scalable process configuration.

Green foundation

1. Triglyceride hydrolysis is carried out in water without added catalysts, organic solvents, or neutralization steps, enabling the direct formation of diglycerides, monoglycerides, free fatty acids, and glycerol without generating byproducts or hazardous residues.
2. Implementation of counter-current heat recovery enables recycling of up to 61% of the process thermal energy, substantially reducing external heating requirements and directly addressing the primary energy-intensity limitation of sub- and supercritical water processes.
3. Residence-time control (0.9–43 s) enables selective enrichment of mono- and diglycerides, producing emulsions with long-term stability comparable to a commercial emulsifier and promoting the release of antioxidant compounds during partial hydrolysis.

1. Introduction

Developing more efficient methods of triglyceride hydrolysis is essential for reducing the use of materials, auxiliary inputs and energy demand in oleochemical production.[1–4] This process enables the formation of free fatty acids, mono- and diglycerides, and glycerol, important intermediates for surfactants, emulsifiers, fuels, and functional additives.[5–10] However, established hydrolysis technologies are hindered by long reaction times, high reagent usage and limited scalability.[11–14]

Conventional acid- and base-catalyzed hydrolysis typically requires stoichiometric quantities of corrosive reagents and generates salt-containing aqueous waste during neutralization (Fig. 1).[15–19] It also operates at residence times of hours.[16,17,19] Although enzymatic hydrolysis offers milder conditions and improved selectivity, its industrial implementation is limited by slow reaction kinetics, enzyme deactivation, high catalyst costs and low space–time yields.[11,13,16,20,21] Consequently, both approaches have inherent limitations in terms of material efficiency, energy demand and process intensification as shown in Table 1.

Hydrothermal processing utilizing subcritical and supercritical water has developed as an alternative method for triglyceride hydrolysis, as water in these states demonstrates a diminished dielectric constant similar to nonpolar solvents, increased diffusivity, and enhanced mass transfer, facilitating ester bond cleavage without the necessity for additional cata-

---

[a] The Institute of Bioeconomy, Department of Chemical Engineering and Environmental Technology, University of Valladolid, Valladolid, 47011, Spain. E-mail: Danilo.Cantero@uva.es
[b] Department of Chemical and Biomolecular Engineering, Cornell University, Ithaca, NY, 14853, USA

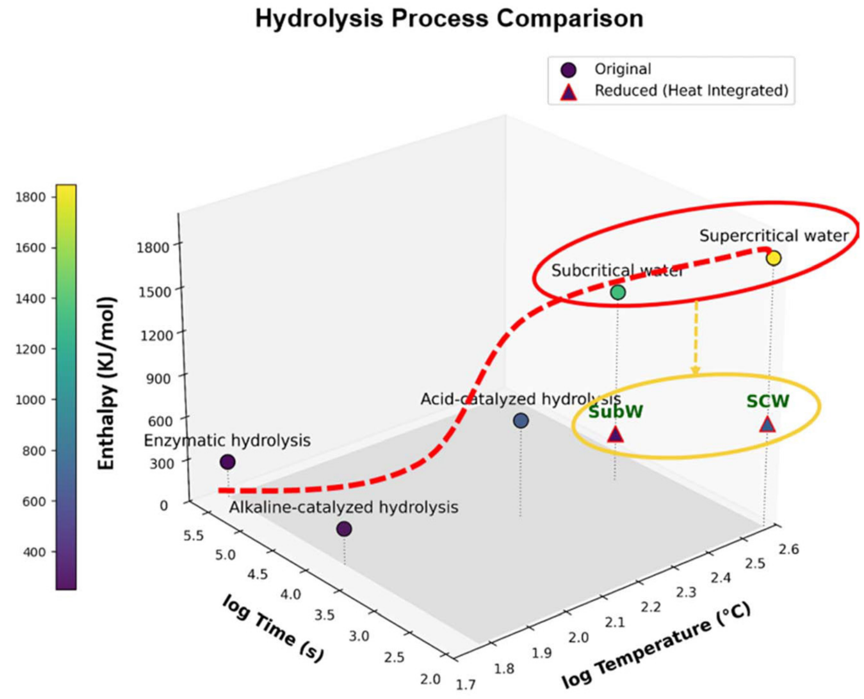

Fig. 1 Three-dimensional comparison of hydrolysis processes based on temperature, reaction time, and enthalpy: real operating conditions (red line) *vs.* target conditions with heat integration (yellow line).

Table 1 Comparison of conventional and hydrothermal routes for triglyceride hydrolysis

Feature	Acid-catalyzed	Base-catalyzed (saponification)	Enzymatic (lipase)	Sub/supercritical water
Reaction time	4–24 h	1–3 h	2–30 h, maximum yield 16 h	Seconds to 1.5 h
Temperature	60–200 °C	60–80 °C	30–50 °C	250–400 °C
Pressure	0.1–1 MPa	~0.1 MPa	~0.1 MPa	10–22.1+ MPa
Catalyst	Solid acids (SO_4^{2-}/ZrO_2, Nafion SAC-13, sulfonated carbons)	Strong base (NaOH/KOH)	Lipase enzyme	None (self-catalyzing)
Solvent/medium	Water or water/alcohol mix	Water/alcohol mix	Water	Water
Yield/conversion	80–98%	~99%	78–98%	90–99%
Downstream separation	Complex; requires neutralization and washing	Requires acidification to release FFA from soap	Simple phase separation; the enzyme is recycled	Simple phase separation upon cooling
Type of vegetable oil	Refined vegetable oils: palm, rapeseed, sunflower, soybean	Waste cooking oil (sunflower-type: 53% oleic)	Coconut oil Canola oil	Sunflower oil
Ref.	15–17	18 and 19	16, 21 and 22	23

lysts or organic solvents.[16,24–30] Previous research has shown that triglycerides can be hydrolyzed into mono- and diglycerides, fatty acids and glycerol under hydrothermal conditions.[13,31–33] However, most of these studies have been performed in batch reactors, where productivity and industrial relevance are limited by discontinuous operation, limited heat transfer, and poor thermal integration.[34–36] Continuous processing has been also explored under subcritical conditions, and systematic studies of triglyceride hydrolysis in continuous supercritical water are still limited.[37–41] In addition, the high thermal input required for supercritical operation necessitates effective energy management to ensure overall process efficiency.[19,23]

The selection of coconut oil in this study was due to its extensive use in cosmetic and personal care formulations and also suitability for the generation of functional glyceride-based ingredients.[1,8,11,42,43] Its triglyceride composition is rich in medium-chain fatty acids and favors the formation of mono- and diglycerides which have a strong amphiphilic character during partial hydrolysis.[44,45] The resulting DG/MG fractions are relevant for cosmetic applications as they exhibit enhanced interfacial activity, improved compatibility with skin and hair, and superior penetration properties compared to intact triglycerides.[8,10,46] Consequently, coconut oil is a valuable platform for evaluating continuous hydrothermal hydrolysis for producing high-performance glyceride fractions.

In this work, a continuous hydrothermal process using water as the reaction medium is investigated for the selective hydrolysis of triglycerides from coconut oil. The study examines whether the combination of ultrashort residence times and continuous operation can enable selective formation of mono- and diglycerides without the use of added catalysts or organic solvents. The process is explored under sub- and supercritical water conditions, with particular attention to the integration of heat recovery as a strategy to reduce the high energy demand associated as a potential improvement point of this technology. In addition, the stability of operation at a pilot scale and the functional performance of the resulting glyceride mixtures are assessed through emulsion stability tests.

2. Materials and methods

2.1. Materials

Type I deionized water (Elix, 10 MΩ cm) was used as the reaction medium. Virgin, unrefined organic coconut oil was commercially sourced (Maxivio, Spain) and used as received. The feedstock consists predominantly of triacylglycerols (TAG; >94 wt%), with minor partial glycerides/free fatty acids typical of commercial coconut oil.[47] Reagents, solvents, standards, suppliers and lot numbers are reported in the SI (section 2.1).

2.2. Supercritical water hydrolysis PHUn-1: the device

Details for the continuous process used to hydrolyze coconut oil in SCW were reported elsewhere.[23,24] The Pressurized Hydrolysis Unit (PHUn-1) shown in Fig. 2 is a custom-designed stainless steel 316L system featuring a sudden expansion reactor (SER) capable of operating at up to 400 °C and 30 MPa. The reactor length (0.09–8.7 m) and flow rates (up to 5 kg h^{-1} water, 2.5 kg h^{-1} oil suspension) are adjustable to control residence times between 0.7 and 43 seconds. A needle valve from Autoclave Engineers model 30VRMM4812-HT enables rapid depressurization (0.1–1 ms) and cooling the reaction mixture from ∼400 °C to ∼150 °C *via* the Joule–Thomson effect and effectively halting further reactions. The reaction time was controlled by changing the total flow rate and the reactor volume.

Water is delivered using a Milton Roy MD140 membrane pump, while the oil suspension is pumped with a Lewa EK1 piston pump. The suspension oil feed remains unheated prior to mixing, ensuring that hydrolysis only begins upon contact with the hot, pressurized water inside the reactor. This prevents secondary reactions and enables precise control of residence time. The reactor configuration (linear or coiled) depends on length, with thermocouples placed for real-time temperature monitoring. An electrical heater inline at nine kilowatts supplies thermal energy to the water stream. A downstream cooler collects the product at room temperature. This system enables precise control of catalyst-free, solvent-free triglyceride hydrolysis with high product selectivity and minimal thermal degradation.

2.3. Supercritical water hydrolysis PHUn-2: pilot scale

The PHUn-2 system operates using the same sample collection procedure and operational methodology as PHUn-1, with the

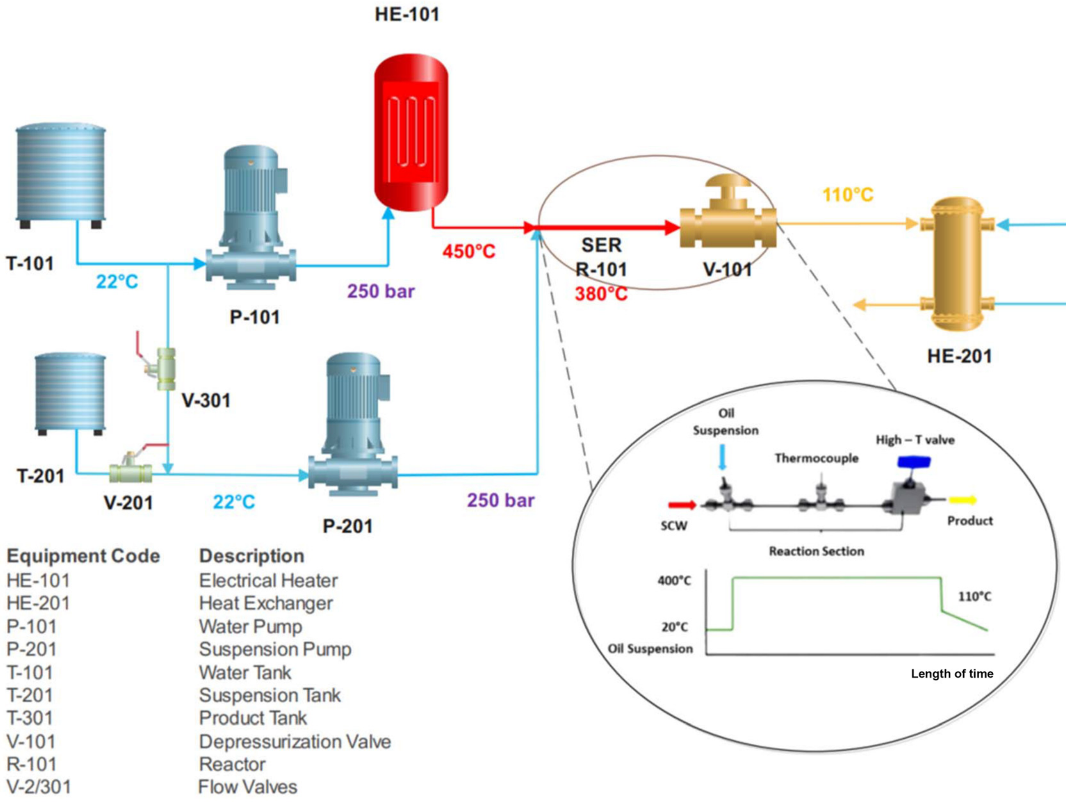

Equipment Code	Description
HE-101	Electrical Heater
HE-201	Heat Exchanger
P-101	Water Pump
P-201	Suspension Pump
T-101	Water Tank
T-201	Suspension Tank
T-301	Product Tank
V-101	Depressurization Valve
R-101	Reactor
V-2/301	Flow Valves

Fig. 2 PFD diagram of the continuous SCW pilot plant.

primary distinction being an increased total feed rate from 7.6 kg h^{-1} to 30 kg h^{-1}. This system is fully automated, ensuring precise control over reaction conditions, flow rates, and product collection. A larger description of this unit can be found in the literature.[48] Additionally, a heat exchanger (H-301) has been integrated into the plant to enhance thermal efficiency and energy recovery and does not affect the process performance.

The heat exchanger consists of an inner tube with dimensions of 6.35 mm × 1.65 mm and an outer tube measuring 19.05 mm × 2.77 mm, with a total length of 6 m. Further details on the system's configuration and operation can be found in section 4.1.

2.4. Experimental design

The experimental setup was designed to explore how changes in water properties affect the hydrolysis of coconut oil, along with examining how the reaction temperature and time impact the process. Table 2 summarizes the tested conditions.

For the hydrolysis of coconut oil, a range of conditions was examined to capture key factors influencing the reaction. Five temperatures (250, 300, 350, 380, and 400 °C) and two pressures (22.0 and 25.0 MPa) were tested across eight different reactor lengths (9, 50, 110, 200, 230, 318, 510, and 870 cm), resulting in varied reaction times. Flow rates were maintained at 4 kg h^{-1} for supercritical water (SCW) and 1.5 kg h^{-1} for the coconut oil mixture, providing a consistent baseline for comparative analysis of hydrolysis under different conditions.

In the 200 cm reactor, the concentration of the coconut oil/water mixture was varied to 10%, 25%, 50%, 75%, and 100% w/w in the tank T-201, corresponding to 3.4%, 8.3%, 17.1%, 25.6%, and 34.2% w/w in the reactor. The goal of this change was the assessment of the concentration effects on hydrolysis yields. For all other reactor lengths, a consistent 50% concentration in the tank was maintained to compare the differences in conversion between the conditions.

Triglyceride conversion was calculated on a mass basis as the fraction of triglycerides consumed relative to the inlet amount. Product yields (diglycerides, monoglycerides, free fatty acids, and glycerol) were defined as the mass fraction of each product formed relative to the initial mass of triglycerides fed to the reactor.

$$X_{\mathrm{TG}}\,(\%) = \frac{m_{\mathrm{TG},0} - m_{\mathrm{TG}}}{m_{\mathrm{TG},0}} \times 100 \tag{1}$$

where X_{TG} is the conversion in percentage on a mass basis; $m_{\mathrm{TG},0}$ is the mass of triglycerides at the reactor inlet; and m_{TG} is the mass of triglycerides at the reactor outlet.

$$Y_{\mathrm{TG}}\,(\%) = \frac{m_{\mathrm{i}}}{m_{\mathrm{TG},0}} \times 100 \tag{2}$$

Y_{TG} is the yield in percentage on a mass basis; m_{i} is the mass of product i measured at the reactor outlet; and $m_{\mathrm{TG},0}$ is the initial mass of triglycerides fed to the reactor.

Table 2 Experimental conditions and pure water properties under those conditions

Temperature (°C)	Pressure (MPa)	Density (kg m^{-3})	Ionic product (pK_{w})	Dielectric constant
250	22	818	11.0	28.1
300	22	738	11.2	21.4
350	25	612	11.6	14.4
380	25	450	12.7	9.3
400	25	166	16.7	3.7

2.5. Characterization of the product

The product composition (TG, DG, MG, total FFA and glycerol) was quantified primarily by high-performance size-exclusion chromatography (HPSEC) following ISO 18395:2012,[49] which enables class-based separation and quantification of glycerides and total fatty acids in complex hydrolysate mixtures. Detailed information on sample preparation, column configuration and analytical conditions is provided in the SI (section 2.5.1). Individual free fatty acids and glycerol were additionally quantified by GC-MS after silylation derivatization using external calibration with authentic standards and an internal standard;[50,51] the full method (derivatization, calibration and instrumental parameters) is reported in the SI (section 2.5.2). FTIR spectroscopy was used to assess functional-group changes between the feedstock and representative products, with acquisition and processing details provided in the SI (section 2.5.3). Total phenolic content (TPC) was determined using the Folin–Ciocalteu assay and reported as gallic acid equivalents as an activity-based proxy for antioxidant-related constituents;[52,53] the assay protocol is given in the SI (section 2.5.4).

2.6. Emulsion preparation and droplet sizing (FlowCam)

Oil-in-water emulsions were prepared from selected hydrolysate products to assess their formulation performance. Emulsification was performed by high-shear homogenization (Ultra-Turrax), and macroscopic stability (creaming/phase separation) was visually screened.[54–56] Droplet size distribution and morphology were quantified by FlowCam 8000 imaging flow microscopy based on automated analysis of droplet images acquired in a flow cell.[57,58] Full formulation matrices, dilution protocols and measurement settings are provided in the SI (sections 2.6.1 and 2.6.2).

2.7. Principal component analysis (PCA) and clustering analysis

Principal component analysis (PCA) and cluster analysis were used to compare samples and group them by compositional similarity, enabling selection of compositionally distinct samples during product development for detailed characterization.

2.7.1 Principal component analysis (PCA). Principal component analysis (PCA) was used to reduce dataset dimensionality and visualize compositional trends.[59] Data were *z*-score standardized prior to analysis. PCA was performed on the covariance matrix of the standardized variables, and samples were projected onto the first two principal components for visualization. Full details are provided in the SI (section 2.7.1).

2.7.2 **Clustering analysis.** To classify samples based on their compositional profiles, *k*-means clustering was applied to the PCA-transformed data.[60] The algorithm partitions data into *k* clusters by iteratively minimizing the within-cluster sum of squares (WCSS). The number of clusters was chosen based on inspection of the WCSS *versus* *k* curve. The clustering results revealed distinct sample groupings, aiding in the interpretation of compositional trends. A detailed description of the clustering procedure, including centroid initialization and convergence criteria, is available in the SI (section 2.7.2).

2.8. Severity factor (i_{ts})

In super-subcritical water (SCW) hydrothermal processing, the severity factor (t_S) is a widely accepted metric for quantifying the combined influence of temperature and reaction time on process kinetics.[61] This study adopts the formulation proposed by Posmanik *et al.*,[62] which normalizes treatment conditions to a reference temperature, allowing for consistent comparison across experimental setups.

The severity factor expresses the equivalent reaction time at a reference temperature T_{ref} of 380 °C and is defined as eqn (3).

$$t_{\text{s}} = t \cdot \exp\left(\frac{T - T_{\text{ref}}}{\omega}\right) \quad (3)$$

where t_{s} is the severity time in seconds, t is the reaction time (s), T is the treatment temperature (°C), and ω is a temperature-dependent empirical parameter. In most studies, ω is approximated as a constant value of 14.75, derived from the Arrhenius relationship as shown in eqn (4).

$$\omega = \frac{{T_{\text{ref}}}^2 \cdot R}{E_{\text{a}}} \quad (4)$$

Here, T_{ref} is the reference temperature (380 °C), while the universal gas constant (R) was taken as 8.314 J mol^{-1} K^{-1}. The apparent activation energy (E_{a}) and other kinetic parameters were derived based on prior work by Minami–Saka,[63] Milliren,[64] Savage[65] and Cocero[23] who also investigated the influence of fatty acids acting as autocatalysis. The development of this kinetic analysis is shown in the SI (section 2.8).

By combining eqn (3) and (4), the final expression used for t_{s} in this study becomes eqn (5).

$$t_{\text{s}} = t \cdot \exp\left(\frac{E_{\text{a}}(T - T_{\text{ref}})}{{T_{\text{ref}}}^2 \cdot R}\right) \quad (5)$$

This formulation enables the comparison of reaction severity across diverse thermal profiles and is instrumental in evaluating and optimizing PDC extraction performance across reactor systems. The kinetic modeling of these reactions and the fitting of the activation energy can be found in section 2.8.1 of the SI.

2.9. Green chemistry metrics

Environmental and process efficiency metrics were studied for the continuous hydrolysis of coconut oil at various residence times. Key green chemistry indicators such as atom economy, *E*-factor, process mass intensity (PMI), reaction mass efficiency (RME), carbon efficiency, and energy intensity (EI)[4,66,67] are reported in the Results section. Further details on the calculation methodology can be found in the SI (section 4.1).

3. Results and discussion

This section is structured to guide the reader through the progressive stages of coconut oil hydrolysis and the characterization of the resulting bio-based products under subcritical and supercritical water conditions. The first part focuses on the hydrolysis process itself, detailing the influence of temperature, pressure, and feed concentration on the conversion of triglycerides and the formation of diglycerides, monoglycerides, free fatty acids, and glycerol. Subsequently, the profiles of individual fatty acids are analyzed to evaluate the reaction pathways and solubility-driven selectivity of hydrolysis products. The second part examines the functional potential of the hydrolysates, including their composition-based classification through principal component analysis (PCA), molecular transformations observed *via* FTIR spectroscopy, and antioxidant activity. Finally, the emulsification performance is assessed through stability testing, droplet size distribution analysis using FlowCam, and comparative evaluations against commercial emulsifiers.

3.1 Hydrolysis of coconut oil

The data presented in Fig. 3 show the conversion of triglycerides (TG) and the yields of diglycerides (DG), monoglycerides (MG), free fatty acids (FFA), and glycerol (G) during the hydrolysis of coconut oil under subcritical and supercritical water conditions. Triglyceride conversion is reported as the fraction of triglycerides consumed relative to the inlet amount, while product yields are expressed on a mass basis relative to the initial triglyceride feed. Graphs (a) and (b) correspond to experiments conducted at 380 °C and 25 MPa and at 300 °C and 22 MPa, respectively, while graph (c) shows the effect of the inlet coconut oil concentration in the reactor. The complete dataset for all investigated conditions is provided in section 3.1 of the SI.

SCW progressively deconstructs coconut oil into its constituent components, with triglycerides (TG) decreasing over time and being converted into diglycerides (DG), monoglycerides (MG), free fatty acids (FFA), and glycerol (G), as reflected in the conversion profiles at different residence times. Under supercritical conditions at 380 °C and 25 MPa (Fig. 3a), the reduced dielectric constant of water enhances the solubility of non-polar triglycerides, accelerating hydrolysis relative to subcritical conditions (Fig. 3b) where the TG solubility remains limited, a behavior widely reported for SCW systems.[23,68] The hydrolysis rate increases markedly at elevated temperatures, particularly around 380 °C, owing to enhanced molecular mobility, increased collision frequency, and improved reactant solubility, which together promote bond cleavage and favor

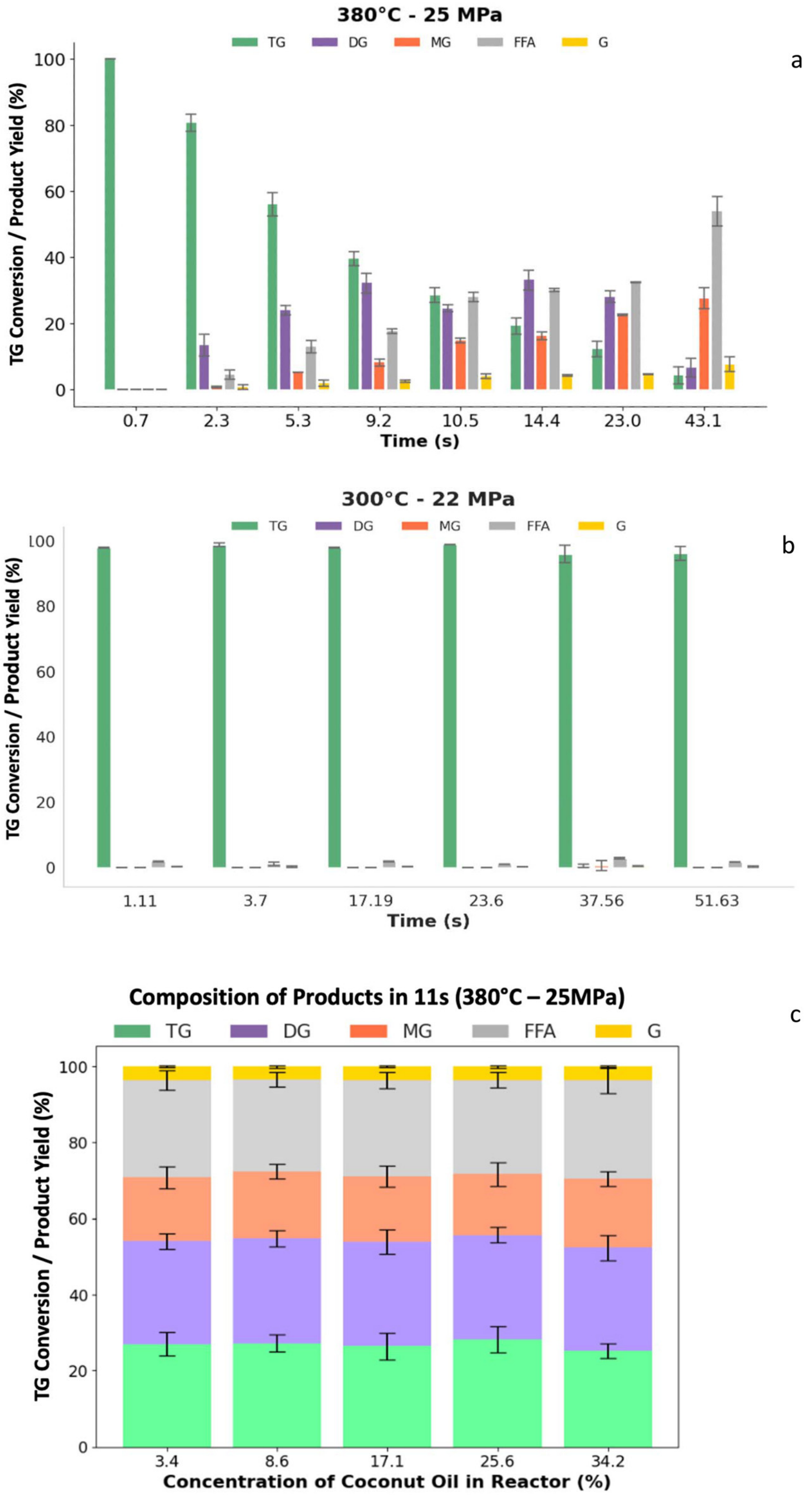

Fig. 3 Coconut oil hydrolysis and product conversion at (a) 380 °C – 25.0 MPa, (b) 300 °C – 22.0 MPa, and (c) 380 °C – 25.0 MPa with different inlet concentrations of raw material (oil) in the reactor.

the formation of DG and MG intermediates.[30,69–71] The dielectric properties of SCW, which vary with temperature and density, further facilitate interactions between water and the hydrophobic regions of triglycerides, thereby governing the hydrolysis mechanism and reaction rate.[23,72]Under these conditions, a residence time of 23 s yielded a product composition of 12 wt% TG, 28.5 wt% DG, 23 wt% MG, 32 wt% FFA, and 4.5 wt% glycerol, indicating a high degree of conversion with

DG and MG as the dominant intermediates. This temperature–pressure combination provides a favorable balance between reaction rate, product selectivity, and energy demand.[23] Detailed experimental conditions for subcritical (250 °C – 220 bar and 350 °C – 250 bar) and supercritical (400 °C – 250 bar) hydrolyses are reported in the SI (section 3.1).

Fig. 3c illustrates the effect of inlet coconut oil concentration on product composition at 380 °C and 25 MPa with a residence time of 11 s. The product distributions (TG, DG, MG, FFA, and G) remain essentially constant as the inlet oil concentration increases up to 34.2 wt%, indicating that the continuous reactor maintains efficient hydrolysis without solubility or mass-transfer limitations. The stable composition across this concentration range highlights the robustness of the system and supports its relevance for scale-up, where higher feed concentrations are desirable to maximize throughput.

In contrast to the present approach, conventional triglyceride hydrolysis typically relies on acid- or base-catalyzed processes that require stoichiometric reagents and downstream neutralization steps, or on enzymatic routes that operate under mild conditions but are limited by slow kinetics and catalyst stability. Batch hydrothermal approaches avoid added catalysts but typically require residence times of minutes to hours and lack continuous operation, constraining throughput and energy management. In contrast, the continuous hydrothermal process investigated here operates at residence times on the order of seconds, without added catalysts or organic solvents, while enabling control over product selectivity through residence-time tuning.

3.2 Profile of fatty acids

The data presented in Fig. 4 illustrate the progression of coconut oil hydrolysis in subcritical and supercritical water at different temperatures (400 °C – Fig. 4a, 380 °C – Fig. 4b, 350 °C – Fig. 4c, and 300 °C – Fig. 4d) and pressures (22–25 MPa). Each figure shows the total concentration of free fatty acids over time and the relative concentration percentages of individual fatty acids, specifically lauric, myristic, and palmitic acids, as well as glycerol. The role of those parameters is to understand the breakdown of triglycerides into various hydrolysis products and observe how temperature influences the reaction kinetics and composition of the resultant compounds.

Fig. 4 presents the behavior of FFAs and glycerol during the hydrolysis of coconut oil in SCW. From this figure, it can be seen that the total FFA content increases more rapidly and attains a higher value at a higher temperature, while the line plots point out the release and accumulation of individual components with time. When the temperature is raised up to 380 °C, the product composition changes very rapidly. These transformations progress at a slower rate at lower tempera-

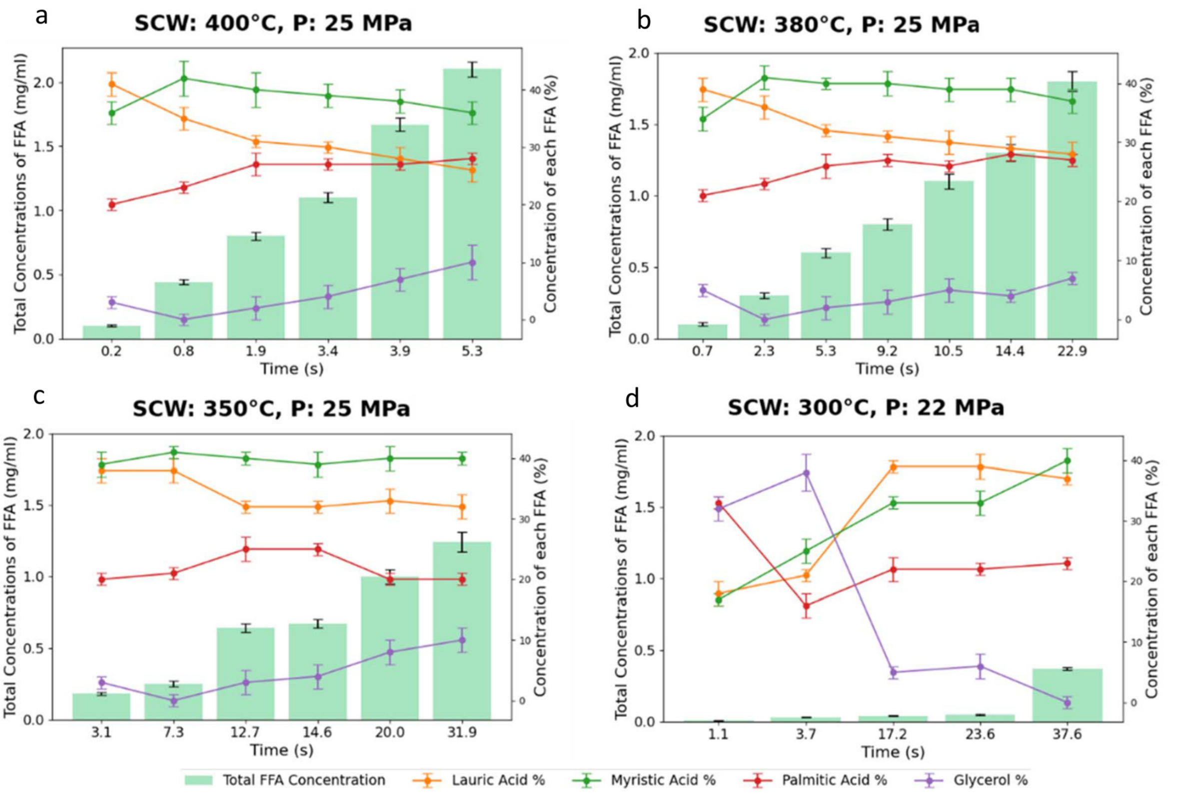

Fig. 4 Fatty acid and glycerol composition (%) on the right axis (y_2) and their total concentration on the left axis (y_1) under different conditions: (a) 400 °C, 25.0 MPa; (b) 380 °C, 25.0 MPa; (c) 350 °C, 25.0 MPa; and (d) 300 °C, 22.0 MPa, over time.

tures, thus confirming the strong temperature dependence of the hydrolysis rate.[23,68]

The evolution of individual FFAs indicates a clear sequence of release during hydrolysis. Lauric acid (C12) dominates the early stages of the reaction, reflecting both its high abundance in coconut oil and its shorter chain length, which facilitates cleavage from the glyceride backbone under supercritical conditions. As the reaction time increases, the relative contributions of myristic (C14) and palmitic (C16) acids gradually increase, suggesting a stepwise hydrolysis mechanism in which ester bonds associated with longer-chain fatty acids are cleaved more slowly due to stronger molecular interactions or less labile positions within the triglyceride structure.[68,73]

The decrease in the relative proportion of lauric acid reflects changes in product composition rather than a decline in its concentration, as additional FFAs are continuously formed during hydrolysis. Glycerol increases steadily under all conditions, consistent with ongoing triglyceride cleavage, while larger compositional fluctuations at intermediate temperatures (Fig. 4d) arise from lower overall hydrolysis yields.

3.3. Statistical analysis

The compositional evolution of the hydrolysis products was assessed by means of principal component analysis (PCA), with the aim of selecting representative samples for further functional analysis. This multivariate technique has been demonstrated to simplify complex datasets while retaining their main variance, thus allowing clear visualization of compositional patterns among samples. The application of PCA to the relative concentrations of triglycerides (TG), diglycerides (DG), monoglycerides (MG), free fatty acids (FFA), and glycerol (G) provides an overview of the changes in product composition that occur throughout the hydrolysis process. This analysis enables classification of samples based on their chemical profiles, independent of processing conditions, and helps identify distinct compositional clusters that correspond to different reaction stages. As shown in Fig. 5, the PCA revealed clear groupings that guided the selection of key samples for further evaluation of emulsification performance and molecular transformations.

Samples exhibiting similar compositions are observed to cluster together, while those with significant differences are spatially separated, thus providing insight into the progression of the hydrolysis reaction, as illustrated in Fig. 5a. The application of cluster analysis resulted in the further stratification of the data into four distinct groups, thereby enhancing the comprehension of compositional differences. Dark blue samples (Cluster 0) are characterized by a high TG content, representing the unreacted or minimally hydrolyzed starting material. Conversely, light blue samples (Cluster 1) exhibited low TG content, indicative of advanced hydrolysis with substantial triglyceride breakdown into smaller components (high amount of FFA). The red cluster (Cluster 2) is indicative of the intermediate stage of the reaction, at which point TG begins to convert into DG and MG. This group exhibits a balance between TG and their breakdown products, reflecting partial hydrolysis. The yellow samples (Cluster 3) are characterized by elevated concentrations of DG and MG, indicative of advanced hydrolysis stages. The compositional diversity observed across the various clusters provides a foundation for the selection of representative samples, which can then be used to evaluate their emulsion properties.

Fig. 5b shows the distribution of samples in different identified clusters. Cluster 0 is the most populated group, holding 38.5% of the total samples, likely to contain the most common compositional features, while cluster 1 accounts for 23.1% of the total samples, comprising the second major grouping; both clusters 2 and 3 have 19.2%, representing smaller and more distinct subgroups. In PCA, as depicted in the figure, the first two principal components, PC1 and PC2, together explain 98.61% of the total variance where 82.39% of the variance is given by PC1 and the remaining 16.22% by PC2; this suggests that the most of the variation within these five major components, namely TG, DG, MG, FFA, and G, is preserved with little loss of information. The legend shows full identifiers of the samples, hence allowing the composition of each cluster to be identified accurately.

Fig. 5c shows a quantitative correlation between compositional clustering and severity time, a kinetic parameter that lumps temperature and residence time into one descriptor. Accordingly, the clustering pattern derived from PCA remains identical even upon normalization to a reference temperature of 380 °C by means of the severity factor. Such consistency ensures that severity time is an appropriate descriptor of hydrolysis development over the wide temperature range tested. A clear trend in compositional change can be seen with the alignment of clusters along increasing severity values—from triglyceride-rich samples at low severities to samples dominated by monoacylglycerols, then diacylglycerols, and finally FFAs at higher severities. This systematic trend confirms the robustness of the unsupervised classification as well as the reliability of the severity factor as a predictive indicator of the hydrolysis extent and product distribution in complex lipid systems.

According to the index of severity, PCA, and cluster analysis, the samples with the greatest deviation are represented as C4, C9, C14, C19, C24, C29, C34, and C40, corresponding to the reaction times of 0.7 s, 2.3 s, 5.3 s, 9.2 s, 14.4 s, 22.9 s, 34.1 s, and 43.1 s, all under constant conditions of 380 °C and 25 MPa.

3.4. Antioxidants and product distribution

The FTIR data in Fig. 6 show the molecular transformations occurring during the hydrolysis of coconut oil under supercritical water conditions, highlighting differences between raw coconut oil (TK111) and hydrolysates at 23 s (C34) and 43.1 s (C40) of reaction.

The antioxidant concentration profile (Fig. 6a), in conjunction with the FTIR analysis (Fig. 6b), reveals a strong correlation between chemical bond cleavage and the liberation of bioactive compounds. Initially, the raw material (0 s) consists predominantly of triglycerides (TG), as evidenced by a strong

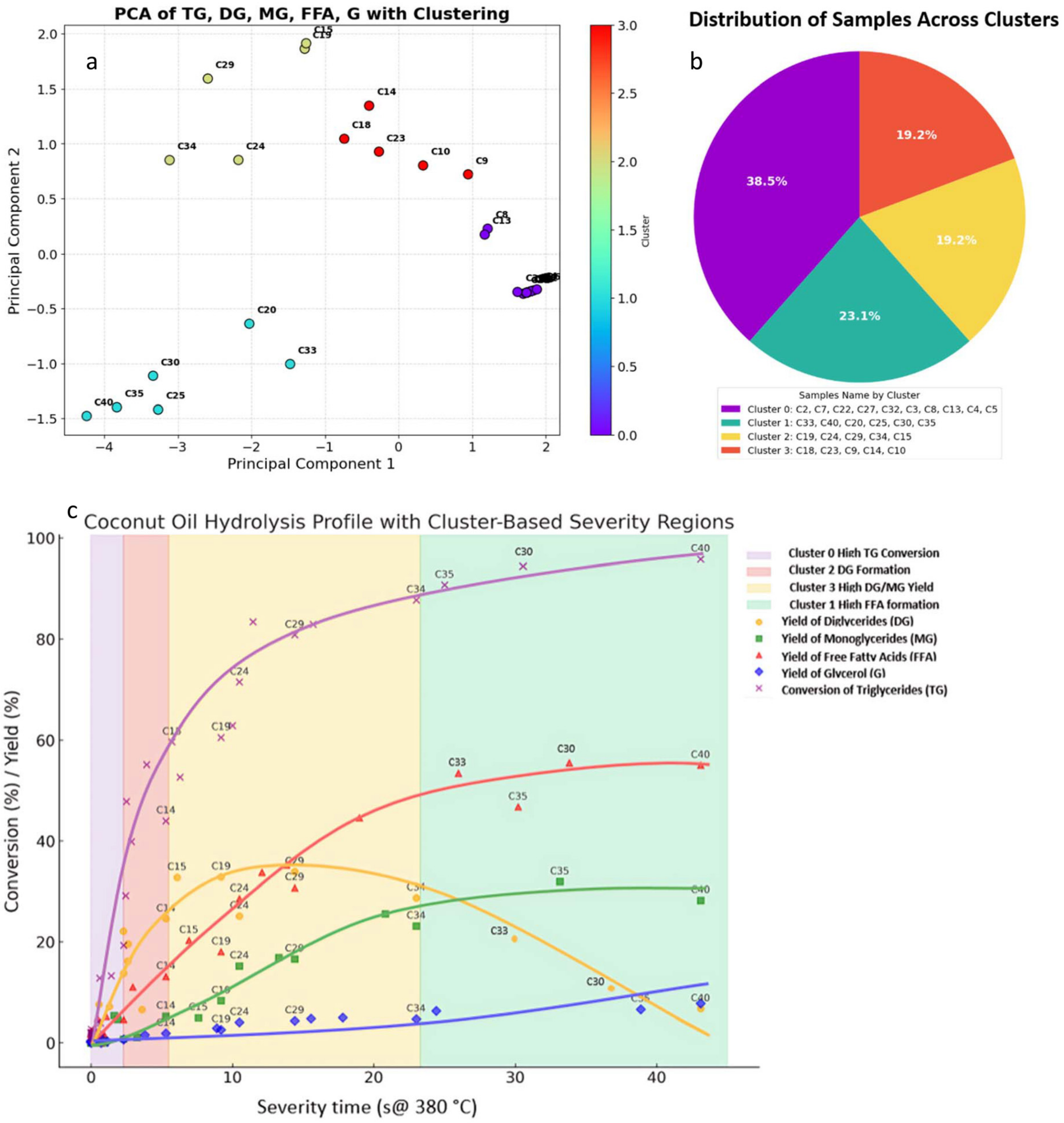

Fig. 5 (a) PCA analysis grouped by clusters, (b) sample distribution across clusters and (c) conversion/yields (%) of products from coconut oil hydrolysis at 380 °C over severity time.

carbonyl (C=O) peak at 1740 cm^{-1} and a strong aliphatic C–H stretching (2800–3000 cm^{-1}) indicative of ester bonds and long hydrocarbon chains.[74] The low antioxidant concentration (590.54 mg L^{-1}) at this stage suggests that most bioactive compounds remain trapped within the oil matrix.

As hydrolysis proceeds, triglycerides are sequentially converted into diglycerides (DG) and monoglycerides (MG), accompanied by the release of antioxidant compounds. At a residence time of 9.2 s, a marked reduction of the carbonyl (C=O) band and increased hydroxyl (–OH) absorption in the FTIR spectra indicate extensive ester bond cleavage and the formation of glycerol and FFAs,[75] coinciding with the highest antioxidant concentration measured (4114.7 mg L^{-1}), corresponding to a sevenfold increase compared to the raw material. At longer residence times, the antioxidant concentrations progressively decrease (3723.1 mg L^{-1} at 14.4 s, 2688.9 mg L^{-1} at 22.9 s, and 2118.6 mg L^{-1} at 43.1 s), despite continued hydrolysis. In the 600–950 cm^{-1} fingerprint region, the ~721 cm^{-1} band is assigned to CH_2 rocking of long alkyl chains, while weaker features reflect overlapping C–H deformation modes.[76] Overall, antioxidants are native bioactive constituents of the unrefined coconut oil (590.54 mg L^{-1}). SCW does not generate these compounds *de novo*; instead, ester-bond cleavage and partial TG hydrolysis release them from the lipid matrix,

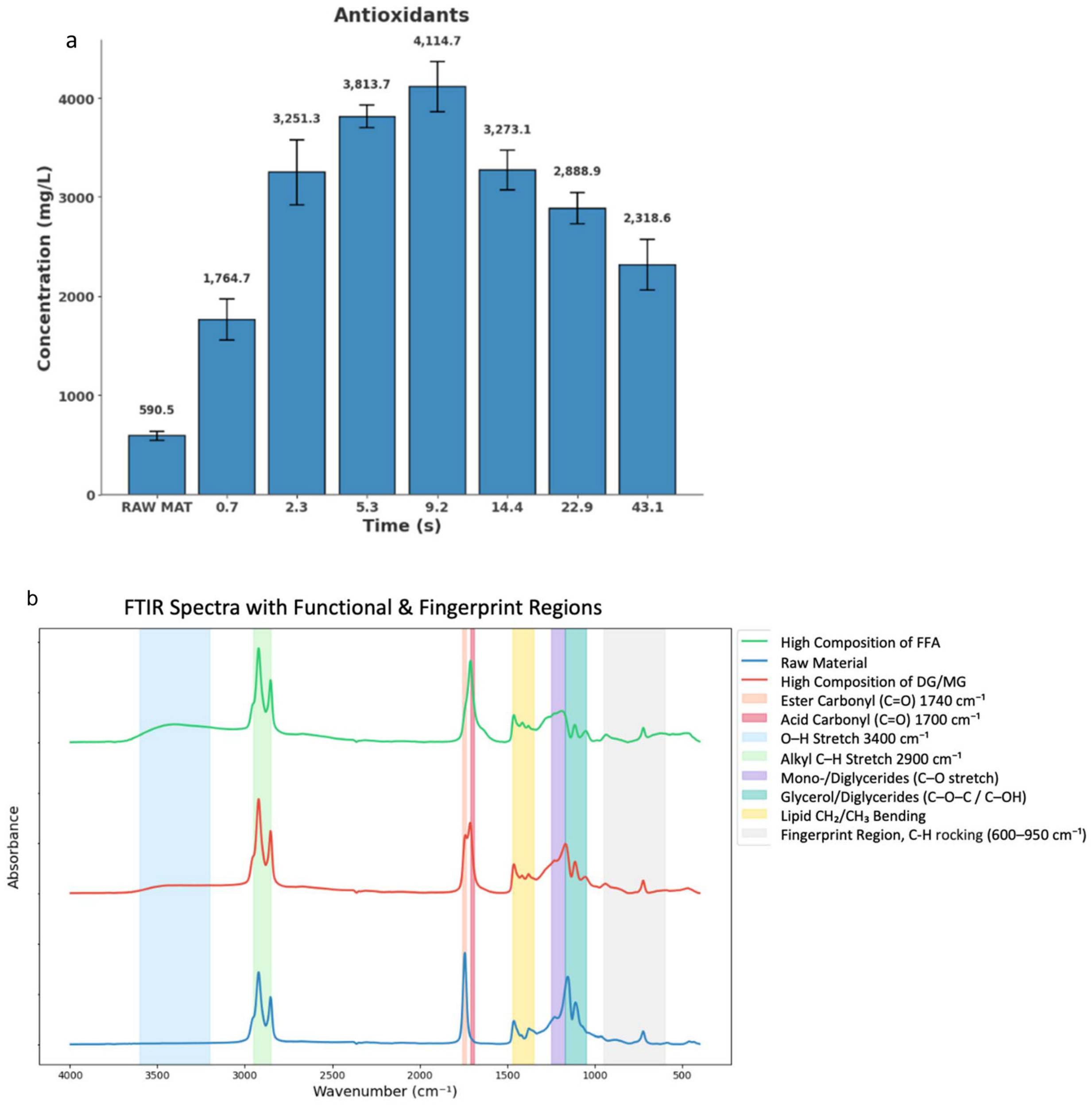

Fig. 6 (a) Total antioxidant compound contents of raw coconut oil and hydrolyzed products over time. (b) FTIR spectra of raw material (raw coconut oil), hydrolyzed product at 22.9 (high composition of DG/MG) s and 43.1 s (high composition of FFA).

giving a maximum of 4114.7 mg L^{-1} at 9.2 s. At longer residence times, the antioxidant level decreases (2118.6 mg L^{-1} at 43.1 s), due to thermal degradation reactions at 380 °C.

The identification of 9.2 s as a critical residence time highlights the strong coupling between molecular structure and antioxidant behavior during hydrothermal processing. Hydrolysates obtained at this stage are enriched in diglycerides and monoglycerides, while limiting extensive conversion to free fatty acids and glycerol, resulting in compositions with favorable amphiphilic characteristics. The simultaneous presence of antioxidant compounds at their highest measured levels further enhances the functional potential of these mixtures. Similar trends of antioxidant release under hydrothermal conditions have been reported for biomass processing;[6,77] however, most studies rely on batch reactors, where prolonged heating and cooling stages obscure precise control of reaction severity.[77] In contrast, the continuous operation employed here enables accurate residence-time control on the order of seconds, demonstrating that controlled partial hydrolysis is essential for tuning product composition and preserving antioxidant compounds in hydrothermal systems.

3.5. Emulsion testing: stability

Emulsions were prepared by mixing 0.2–2 mL of hydrolysate with 2 mL of water to assess the emulsifying performance of the products as a function of hydrolysis composition. Emulsion stability was monitored over time to evaluate resistance to phase separation and to identify hydrolysis conditions leading to effective bio-based emulsifiers. Samples with low diglyceride and monoglyceride contents (C4 and C9) did not form stable emulsions (Fig. 7a), whereas samples enriched in these amphiphilic components (C19, C29, C34, and C40) yielded stable emulsions. Among them, sample C34 exhibited the highest stability after one day (Fig. 7b), consistent with its elevated DG and MG content.

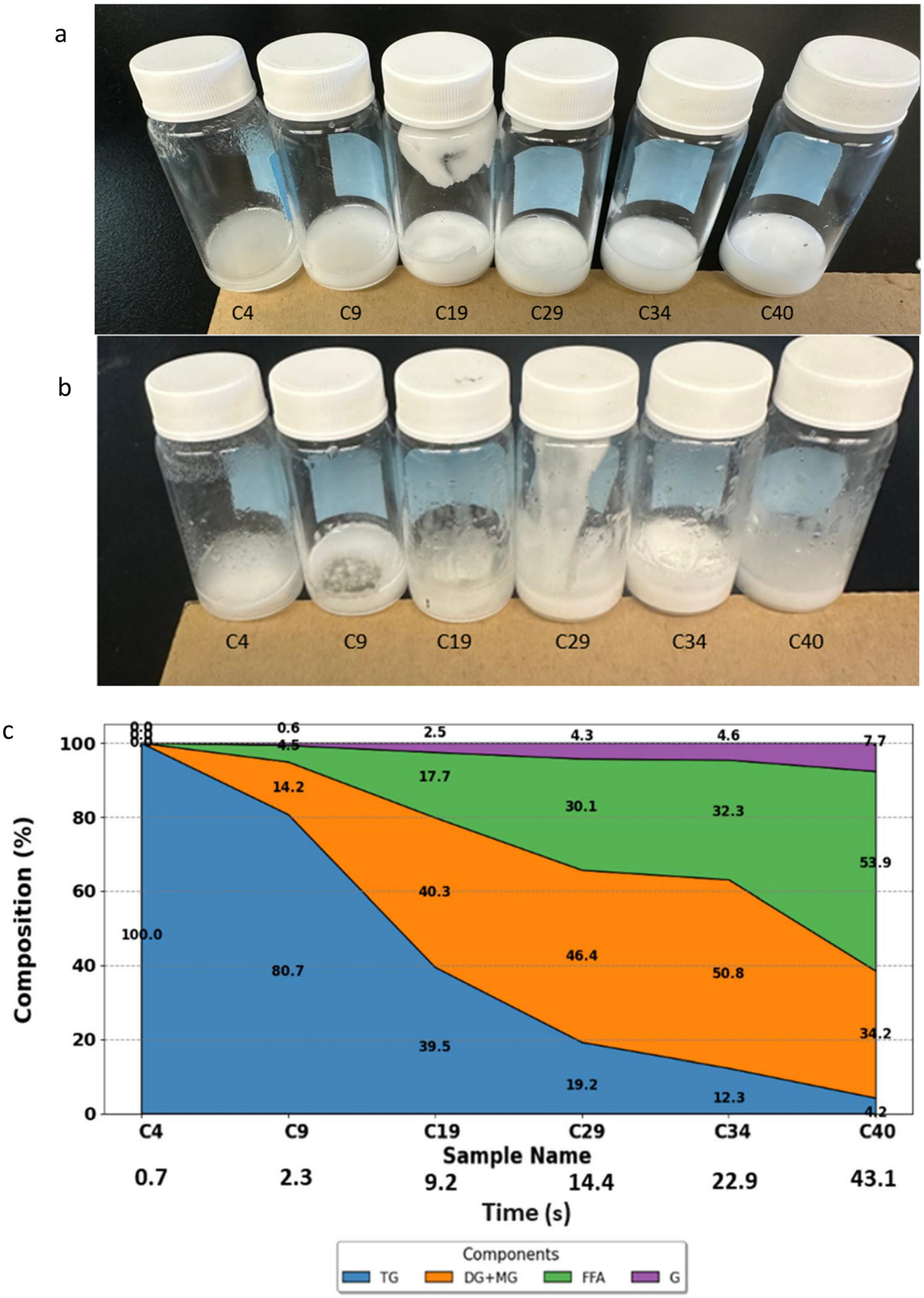

Fig. 7 Images of emulsions highlighting the conditions that successfully form emulsions and the extent of phase separation observed after storage at 25 °C for (a) 1 day and (b) 1 month and (c) distribution of hydrolysis products (TG, DG + MG, FFA, and G) in different residence times and 380 °C, 25 MPa.

During one month of storage (Fig. 7b), pronounced differences in emulsion stability could be seen: samples C4 and C9, which did not create emulsions at first, remained as two distinct phases of oil and water. In the initial steps of analysis, samples C19 and C40 the starting point of the emulsion showed some temporal instability, represented by partial coalescence and phase separation. Samples C29 and C34, on the other hand, showed stability with minor separations, maintaining a creamy appearance. This reveals the importance of the DG and MG fractions to the temporal stabilization of emulsions, through their amphiphilic nature, reducing interfacial tension and preventing droplet coalescence.[78,79] It became evident that sample C34 presents exceptional stability, reflecting the key role of hydrolysis progress in optimizing the emulsified composition toward temporal stability.

From the composition point of view, the differences in emulsion stability among samples are dependent on their composition. Samples C4 and C9 have high levels of TG with very small contents of DG and MG, thus lacking enough amphiphilic molecules at the oil–water interface to stabilize these droplets. In contrast, samples C19, C29, C34, and C40 had progressively higher DG and MG contents and hence showed an improved emulsifying ability (Fig. 7c). Among them, sample C34 showed the maximum stability due to its optimal balance of DG and MG, resulting in a good effect on both the emulsification and strong interfacial stability.

3.6. Emulsion testing: FlowCam

In order to understand the factors governing emulsion stability, the droplet size distribution of emulsions prepared from hydrolyzed coconut oil was analyzed using FlowCam. The influence of the product composition, additive presence, mixing conditions, and formulation environment on droplet formation and stability was systematically examined. This analysis clarifies how di- and monoglyceride content and processing conditions affect emulsion structure and performance, providing practical insight into the formulation of effective bio-based emulsifiers.

3.6.1. Effect of composition on emulsion stability. For this analysis, the emulsion samples were prepared by dispersing 0.5 g of the emulsion in 100 g of water. Emulsion stability was evaluated through measurement of the equivalent spherical diameter (ESD) distribution using FlowCam 8000. The results indicate that samples C4 and C9 produced smaller droplets, with mean diameters of 23.68 μm and 27.91 μm, respectively, but exhibited rapid instability over time (Table 3). This behavior is likely attributable to diminished surfactant activity or inadequate interfacial interactions, precipitating phase separation. Conversely, samples C19 and C29 initially formed emulsions but underwent gradual destabilization over time, indicative of a partial breakdown of the emulsion structure.

Conversely, emulsions containing C34 and C40 depicted larger mean ESD values of 51.8 μm and 47.4 μm, respectively, with enhanced stability. The results obtained suggest that higher concentrations of diacylglycerol (DG) and monoacylglycerol (MG) in C34 contribute to the creation of larger droplets of the dispersed oil phase in the fluid phase, likely due to stronger interfacial tension reduction. As illustrated in Table 3, there is a clear correlation between droplet size and emulsion stability, as evidenced by the data for the particle size distribution for all samples.

The histogram shown in Fig. 8 illustrates the distribution of particle sizes (Diameter (ESD) [μm]) for sample C34, where the *x*-axis represents particle size and the *y*-axis shows frequency. This figure presents the particle size distribution for C34, a sample that demonstrated superior emulsion stability. The higher frequency of larger droplets and the reduced number of sub-20 μm particles indicate stronger droplet integrity and resistance to phase separation.

3.6.2. Effects of additives and conditions on particle size and stability. For FlowCam analysis, emulsions were prepared by dispersing 0.5 g of emulsion in 600 g of water, a dilution ratio selected to ensure adequate dispersion and minimise droplet overlap during measurement. The effect of stabilisers

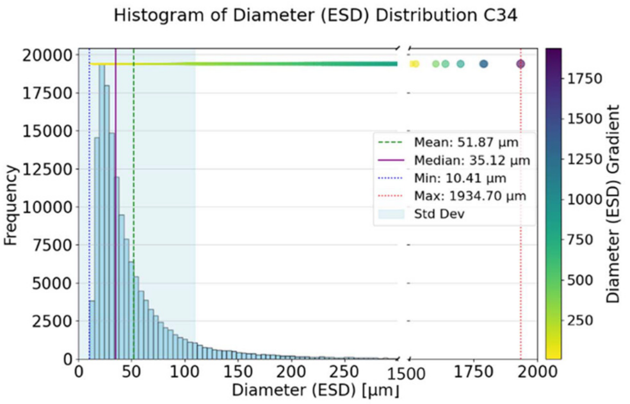

Fig. 8 Histogram of diameter (ESD) distribution for sample C34.

Table 3 Particle size distribution of emulsions dissolved in 100 g of DI water

Sample	Mean (μm)	Median (μm)	Max (μm)	Stability observation
C4	23.6 ± 1.9	20.6 ± 1.7	137.3 ± 5.6	Unstable, rapid phase separation
C9	27.9 ± 2.2	25.5 ± 1.9	142.5 ± 6.2	Unstable, poor interfacial tension control
C19	37.5 ± 2.5	31.7 ± 2.2	205.4 ± 8.4	Initial emulsion, later breakdown
C29	40.2 ± 3.0	33.3 ± 2.4	324.1 ± 12.5	Moderate stability, slight coalescence
C34	51.9 ± 2.8	45.0 ± 2.3	193.4 ± 7.6	Most stable, suitable for emulsions
C40	47.5 ± 2.6	42.9 ± 2.2	186.9 ± 7.4	Stable, retained emulsion structure

was evaluated using hydrolysed coconut oil sample C34_600 with the addition of cetearyl alcohol (2%) and xanthan gum (0.5%). In the absence of additives, the emulsion exhibited a mean droplet diameter of 33.9 µm, with droplets up to 259.8 µm, and showed only moderate stability. Upon incorporation of stabilisers, the mean droplet size decreased to 27.1 µm, accompanied by a narrower size distribution and improved homogeneity, as illustrated in Fig. 9a. This behaviour is consistent with enhanced interfacial stabilisation, which limits droplet coalescence and improves dispersion stability under ambient conditions.

The emulsification process was further subjected to variable mixing speeds 10 000 rpm and 20 000 rpm by means of an Ultraturrax homogenizer. At a rotational speed of 10 000 rpm, the emulsions reached a mean droplet size of 27.12 µm and showed excellent stability. The moderate shear rate was sufficient to form small, uniform droplets without structure breakdown. On the other hand, at a speed of 20 000 rpm, an increase in droplet size was observed with a mean of 31.76 µm, accompanied by a broader size distribution, leading to only moderate stability (Table 4). This reflects that while high levels of shear can enhance the initial droplet disruption, it may also cause coalescence because of interface disruption with incomplete coverage by the stabilizer. Thus, although higher energy input offers better initial dispersion, it may result in lower long-term stability of the emulsion due to secondary interactions among droplets.

Temperature was shown to be a critical factor affecting the performance of emulsification. When the process was conducted at 50 °C, the average droplet size reduced significantly, reaching as low as 19.5 µm, which evidenced the production of finer and more stable emulsions. Such an improvement can be attributed to the increased viscosity reduction of the oil phase and the enhanced diffusion of the emulsifying agents at higher temperatures, in which both factors support efficient droplet disruption and more effective interfacial stabilization, respectively. Compared to commercial Lecithin–Tween emulsions this achieves a finer size with better stability. During the present study, emulsions produced at 50 °C were shown to possess the highest degree of stability; this confirms the hypothesis that moderate thermal input greatly promotes the efficiency of emulsification in bio-based systems.

The emulsions were then subjected to testing under a different ionic strength and pH to assess the influence of environmental conditions. The addition of 10% (w/w) calcium chloride ($CaCl_2$) increased the average droplet size to 32.4 µm, indicating some degree of destabilization. This is attributed to the fact that Ca^{2+} ions compress the electrical double layer at the oil–water interface, reducing electrostatic repulsion among droplets, hence enhancing aggregation. However, the maximum droplet size remained well below that of the untreated emulsions, suggesting that the Ca^{2+} ions probably act as bridging agents among droplets, leading to partial, but not complete, destabilization.

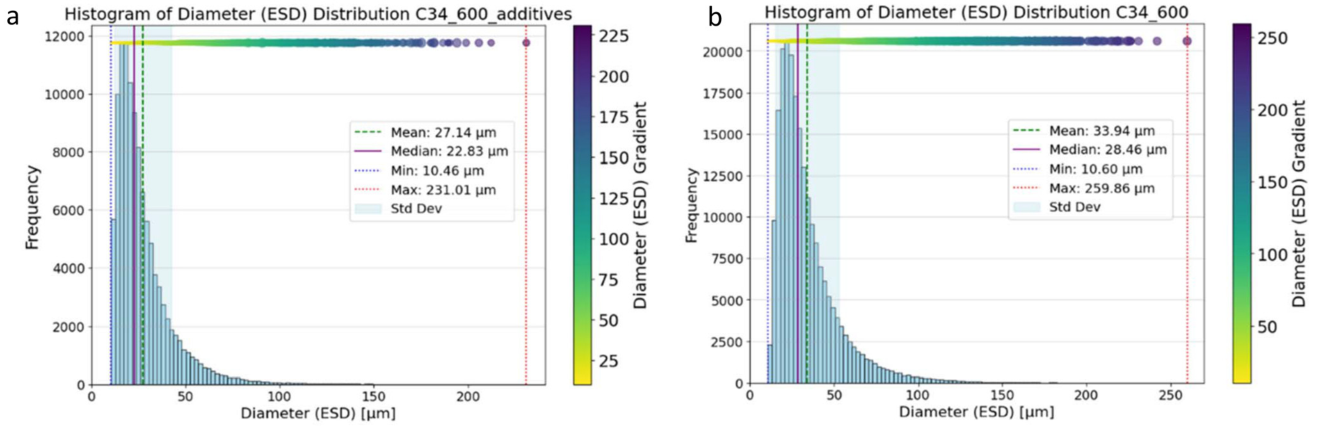

Fig. 9 Histograms of diameter (ESD) distribution for sample (a) C34_600_additives and (b) C34_600.

Table 4 Particle size distribution of emulsions dissolved in 600 g of DI water

Sample	Condition(s)	Mean (µm)	Median (µm)	Max (µm)	Stability description
C34_600	25 °C (no additives)	33.9 ± 2.5	28.4 ± 2.1	259.8 ± 10.3	Moderate stability
C34_600_additives	25 °C + stabilizers	27.1 ± 1.8	26.4 ± 1.7	210.9 ± 8.5	Improved stability
C34_600_additives_10K rpm	10 000 rpm	27.1 ± 1.5	25.9 ± 1.4	194.2 ± 7.1	High stability
C34_600_additives_20K rpm	20 000 rpm	31.8 ± 2.1	26.6 ± 1.6	232.4 ± 9.4	Moderate stability
C34_600_additives_50 °C	50 °C	19.5 ± 1.2	18.0 ± 1.1	87.4 ± 4.2	Best stability
C34_600_additives_$CaCl_2$	10% w/w $CaCl_2$	32.4 ± 2.3	28.8 ± 1.9	152.2 ± 6.3	Moderate stability
C34_600_additives_acidic	pH = 4	30.0 ± 2.0	27.8 ± 1.7	178.0 ± 7.5	Reduced stability
Lecithin–Tween emulsions[80]	25 °C	25–42	0.1	70	Stable

Under acidic conditions (pH 4), the particle size of emulsions was at an average of 29.8 µm and showed reduced stability. This reduced electrostatic repulsion is because protonation of polar headgroups on these emulsifiers prevents them from doing their job of keeping droplets apart. Although the largest droplet size (178 µm) was smaller when compared to the unmodified emulsion, the overall destabilization brought out the system's sensitivity to changes in interfacial chemistry due to pH alteration.

3.7. Separation of fatty acids from glycerides and compared with commercial emulsifiers

To assess the functional role of di- and monoglycerides (DG and MG) in emulsion stabilisation, free fatty acids (FFAs) were selectively removed from the hydrolysate by extractive separation. This step aimed to enhance interfacial performance by reducing excess FFA, which can interfere with emulsion stability, while preserving the DG/MG fractions responsible for interfacial activity. The treated product was subsequently evaluated against a commercial-type emulsifier under stress conditions, including centrifugation, as a measure of interfacial strength and emulsion integrity. FFA separation was achieved *via* stoichiometric neutralisation using a 1 M NaOH solution, optimised to minimise losses of DG and MG. Under these conditions, the FFA content was reduced by 16% with only minor depletion of the DG and MG fractions.

A comparative stability test was conducted in order to evaluate the performance of the formulated emulsion (comprising 61% water, 14% hydrolysate and 25% oil) against a commercial reference emulsifier, SUPER JILK (Lot No. 6102625). The assessment of emulsion stability was conducted through a centrifugation process at a speed of 3000 rpm for a duration of 3 minutes. As shown in Fig. 10a, the commercial sample displayed evident phase separation into three discrete layers, indicative of minimal resistance to centrifugal stress. In contrast, the emulsion formulated with the coconut oil hydrolysate demonstrated homogeneity post-centrifugation (Fig. 10b), thereby indicating an enhancement in resistance to coalescence and phase separation. This enhanced stability is consistent with the selective enrichment of di- and monoglycerides and the reduced free fatty acid content of the hydrolysate. The formulated emulsion has demonstrated stability for a period of up to six months when stored under ambient conditions, with ongoing investigations focused on assessing its long-term stability.

4. Energy integration as a key enabler for scalable supercritical hydrolysis

The shift of supercritical water hydrolysis (SCWH) processes from a lab setting to an industrial scale requires effective energy management, where heat recovery systems are crucial for enabling ongoing high-temperature operations. At first, the incorporation of a heat exchanger was avoided by the group because the very short residence times required for converting simple model compounds like glucose[81] or lignocellulosic biomass[82,83] meant that even slight delays caused by additional equipment could jeopardize product selectivity.[82] At that stage, rapid quenching *via* an expansion valve and the Joule–Thomson effect was preferred to preserve reaction specificity. However, as the process transitioned toward the hydrolysis of different substrates, such as esters, which require longer reaction times—up to 43.1 seconds in this study—became necessary, thereby allowing for thermal integration without detrimental effects on selectivity. This advancement enabled the successful incorporation of an advanced heat exchanger (HE-301) into the upgraded PHUn-2 system. The utilisation of heat recovery and reuse in the process stream has been demonstrated to engender a reduction in external energy input of over 50%. This enhancement of process sustainability paves the way for stable, scalable, and economically viable bio-based production.

Fig. 11 presents the upgraded PHUn-2 system, an advancement over the PHUn-1 setup, designed for supercritical water (SCW) processing in oil–water mixtures. The operational structure stays aligned with PHUn-1, but there is a significant rise in flow rate capacity, now at 30 kg h^{-1}, comprising 20 kg h^{-1} of water and 10 kg h^{-1} of oil. This represents a notable enhancement from the 7.6 kg h^{-1} overall flow rate in the earlier setup. The oil concentration in the reactor is 33.3% w/w, ensuring a high productivity, smooth, controlled, and stable pumping

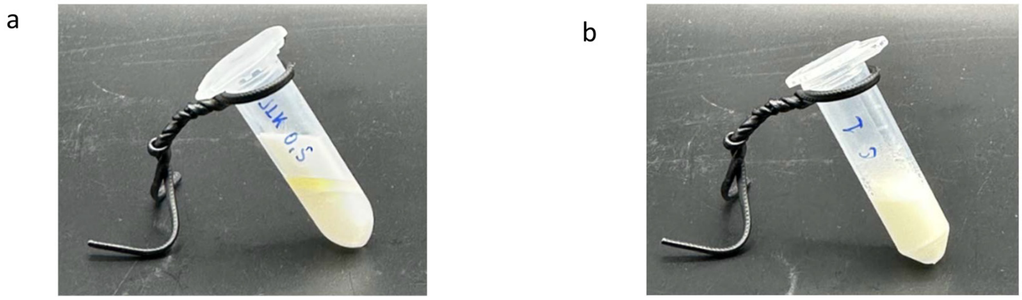

Fig. 10 (a) The emulsion obtained from SUPER JILK following centrifugation exhibited phase separation, as illustrated. (b) The emulsion stability of the Coco sample remained unchanged following centrifugation.

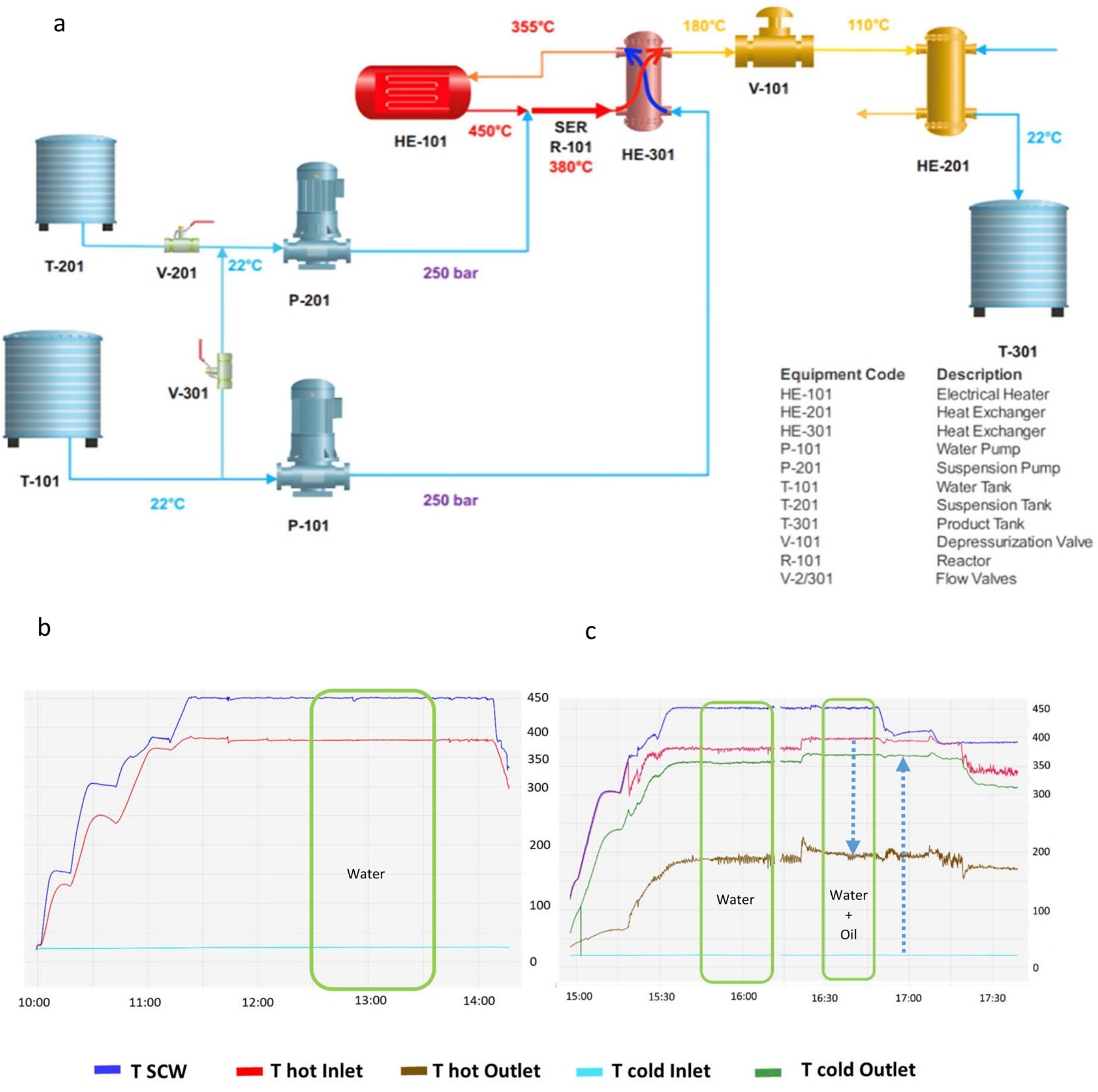

Fig. 11 (a) Process configuration and energy integration in PHUn-2; and profiles of the temperatures (b) without heat integration and (c) with heat integration.

process that maintains a steady operational regime throughout the system. The primary enhancement in PHUn-2 is the addition of another heat exchanger, HE-301, which is vital for optimizing energy efficiency and enhancing temperature stability. The countercurrent concentric tube heat exchanger (HE-301) enables heat recovery and preheating prior to the flow entering the main electrical heater (HE-101). This leads to a significant decrease in the need for heating energy. The system reaches an outlet temperature of 355 °C when only water is circulated and 370 °C with an oil–water mixture (33% w/w oil), which is due to the greater specific heat capacity (C_p) of oil relative to water.

HE-301 is a countercurrent heat exchanger in which the cold stream enters at 22 °C and leaves at 355 °C for the water-diluted slurry (or at 370 °C for the oil–water mixture); meanwhile, the hot stream heating up is at 380 °C for water and at 397 °C for the oil–water mixture, while it exits at approximately 190 °C for both occasions. The purpose of this heat exchanging is, with the efficient energy transfer, to minimize thermal loss and heat stress on the primary heater (HE-101).

Fig. 11b shows the temperature profiles for different process conditions. The blue line represents the temperature of the supercritical water (SCW), while the red line corresponds to the temperature of the oil–water mixture without the implementation of HE-301. Without heat recovery, the system demands a higher energy input to reach the desired operational temperature, leading to increased energy consumption.

In comparison, Fig. 11c and 12b highlight the benefits of energy recovery with HE-301 under the same operating con-

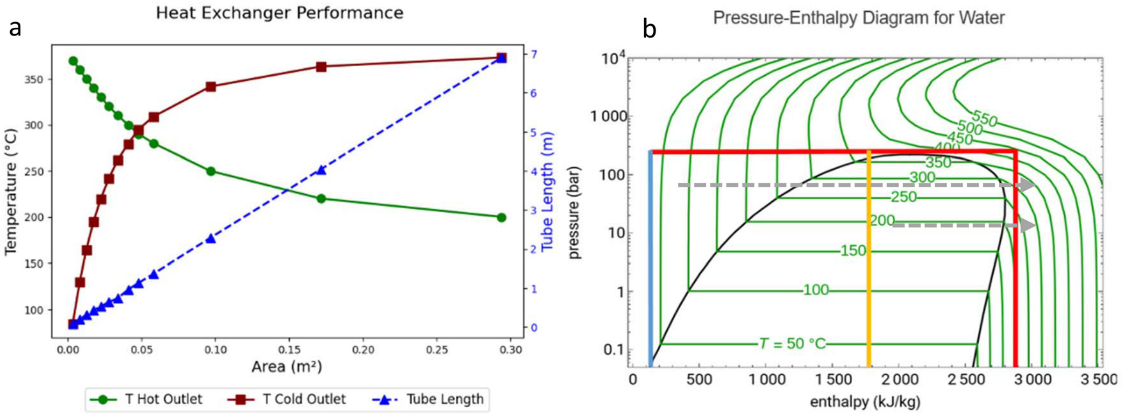

Fig. 12 (a) Effect of heat exchange area on outlet temperatures and tube length in a heat exchanger system, and (b) pressure–enthalpy diagram illustrating the energy required to heat water from 22 °C to 450 °C (blue to red line) and from 370 °C to 450 °C (orange to red line) using HE-301.

ditions. The overall enthalpy required to heat up 20 kg h^{-1} of the stream to 450 °C is approximately 2955.44 kJ kg^{-1}. However, through effective energy integration, the system recovers up to 1786.5 kJ kg^{-1} for the oil–water mixture and 1660 kJ kg^{-1} for the water-diluted slurry. This represents a substantial saving in external energy utilization by drawing effectively on the residue heat of the exiting stream to heat up the cold feed.

The result through the implementation of energy balance shows that HE-301 installation decreases the energy consumption by 55% for water-diluted slurry processing and by 61% for oil–water mixture processing. It is clear from this that adding heat into the system makes a huge difference in general energy efficiency. This now makes PHUn-2 a more feasible and energy-efficient configuration toward supercritical water processing applications.

Fig. 12 shows the correlation among heat exchange area, the outlet temperatures of both hot and cold fluids, and tube length, offering an in-depth examination of the heat exchanger's thermal performance. The SR-Polar thermodynamic property approach was employed in Aspen Plus for modeling the supercritical heat exchanger, as it integrates the Soave–Redlich–Kwong equation of state with polar interaction adjustments, making it effective for precisely forecasting the phase behavior, enthalpy, and various thermophysical properties of polar or associating substances in supercritical and significantly non-ideal scenarios.

The heat exchange area (m^2), displayed on the *x*-axis (Fig. 12a), is an essential element influencing heat transfer efficiency. As the available surface area increases from 0 m^2 to 0.3 m^2, enhanced thermal contact between the fluids leads to improved heat exchange. The temperature of the hot outlet (green line) shows a downward trend, dropping from 380 °C to 200 °C, reflecting increased heat dissipation as the heat exchange area enlarges. On the other hand, the cold outlet temperature (red line) shows a rising trend, climbing from 83.9 °C to 370 °C, indicating enhanced energy absorption by the cold stream as a result of the expanded heat exchange surface. The length of the tube (blue dashed line), displayed on the secondary *y*-axis, grows in proportion to the heat exchange area, varying from 0.08 m to 6.9 m.

A temperature deviation of 20 °C is observed between the calculated and experimental values, which is primarily attributed to heat loss due to insulation inefficiencies. This loss occurs as the heat exchanger tube extends up to 6 m, which increases the potential for thermal dissipation into the surroundings. The heat exchanger dimensions include an outer tube measuring 19.05 mm × 2.77 mm and an inner tube measuring 6.35 mm × 1.65 mm. Within this system, the hot stream flows through the smaller inner tube, while the cold stream, which subsequently experiences a temperature increase, passes through the larger outer tube.

Fig. 13 shows the percentage reduction in external energy consumption achieved at various pre-mixing water temperatures in the hydrolysis process. The temperatures shown represent the temperature of the water stream before mixing with coconut oil—not the actual reactor temperature. The data compare two feed types: oil–water mixtures and water-diluted slurries. The highest energy savings, reaching 74%, are observed at a water inlet temperature of 380 °C, with a corresponding reactor temperature of approximately 320 °C. Although approximately 61% energy savings were achieved at 450 °C—slightly below the optimal threshold—operating under supercritical water (SCW) conditions remains essential for maximizing the product selectivity, quality, and overall reaction performance. While supercritical conditions remain favorable, the subcritical regime, particularly around 380 °C, offers the most energy-efficient operational window for preheating, which can open a new alternative for fully hydrolyzed triglycerides and use those fatty acids as raw materials for biofuels.

5. Toward a zero-waste biorefinery: valorization of all product streams

Following hydrolysis, the product mixture can be refined into different products as depicted in Fig. 14. The product first

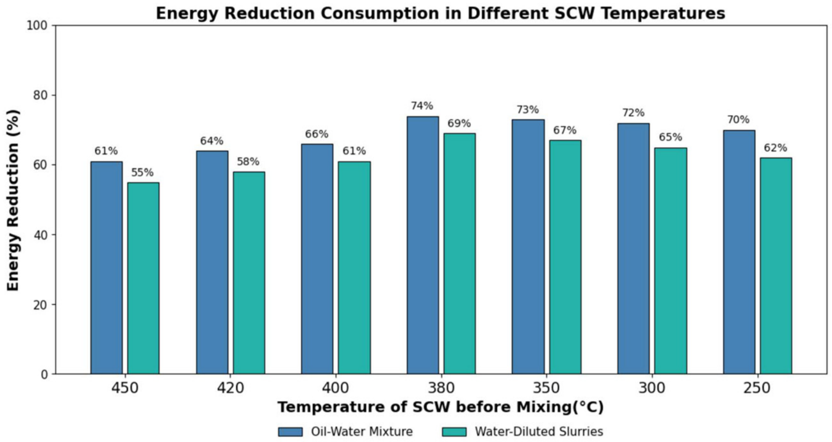

Fig. 13 Energy savings as a function of water temperature before mixing under super-subcritical operation.

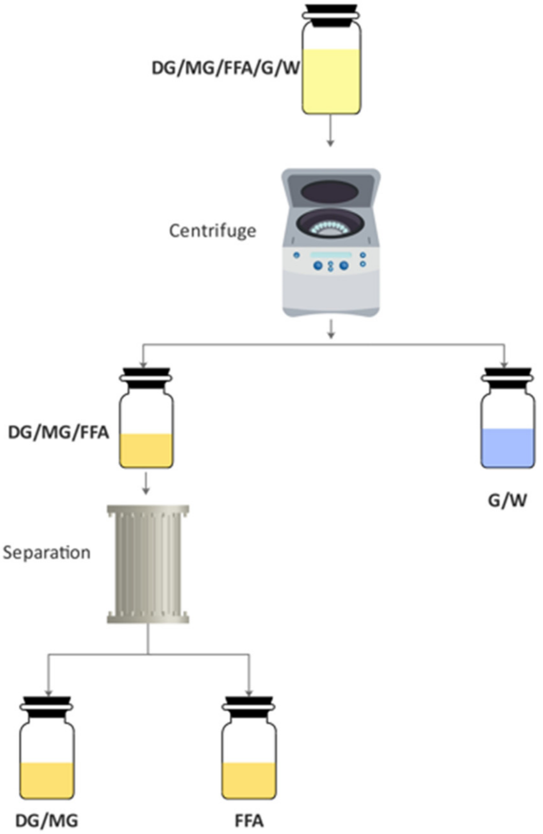

Fig. 14 Closing loop: recovery and utilization of hydrolysis products.

decants into a light-organic phase with FFAs, MGs, DGs, and residual triglycerides, and a heavy-aqueous phase rich in glycerol and water. High-purity FFAs are recovered *via* alkaline neutralization,[84] vacuum or short-path distillation (>99% purity),[85] organic solvent nanofiltration (OSN),[86] supercritical CO_2 extraction,[87] or adsorptive separation using ion-exchange resins.[88] FFAs are utilized as precursors for soaps and detergents[89] and as feedstocks for fatty alcohols, esters, and amines in surfactants, lubricants, and coatings.[90] Medium-chain FFAs, especially lauric acid, exhibit antimicrobial properties and serve as renewable sources for biofuels and biopolymers.[91] The glycerol–water mixture is directly applied in fermentations, anaerobic digestion,[92] microalgae cultivation, and heat-transfer fluids and also functions as a cryoprotectant,[93] a viscosity modifier, and a water activity (A_w) regulator in food, chemical, and pharmaceutical formulations.[94]

5.1 Green chemistry metrics of continuous hydrolysis of coconut oil

Table 5 summarizes the environmental and process efficiency metrics for the continuous hydrolysis of coconut oil in supercritical water at different residence times. Atom economy, process mass intensity (PMI), reaction mass efficiency (RME), *E*-factor, carbon efficiency, and energy intensity (EI) are reported.[4] The calculation methodology and the complete mass balances for base-, acid-, and enzymatic triglyceride hydrolysis are provided in section 4.1, Table S2 of the SI. For consistency across the cited literature, the triglyceride feed was normalized to 100 g for all acid-, base-, and enzymatic hydrolysis routes, enabling a direct and transparent comparison of the green metrics. Water recycling is included in the calculations in Table 5 (70% recovery), but the green metric without water recycling is shown in Table S3 in section 4.1 of the SI.

All green metrics improve systematically with increasing residence time, reflecting the transition from partial to near-quantitative hydrolysis. At 23 s, the process reaches an optimal balance between diglyceride/monoglyceride selectivity, material efficiency, and energy performance, achieving a high atom economy (90.7%) and efficient conversion of the feedstock into value-added products, including fatty acids, partial glycerides, and glycerol, recovered as co-products. Under these conditions, the high RME (0.74), low *E*-factor (0.35), and PMI (1.35) indicate minimal material losses. The energy intensity decreases markedly with residence time and is further reduced through heat integration, reaching 3.6 MJ kg^{-1}.

Table 5 Environmental impact metrics over time and compared with other hydrolysis methods

t (s)	Atom economy (%)	PMI	RME	*E*-Factor	EI (MJ kg^{-1}) without HE	EI (MJ kg^{-1}) with HE	Ref.
2.3	20.8 ± 0.5	6.1 ± 0.18	0.16 ± 0.05	5.1 ± 0.15	41.8 ± 1.22	16.3 ± 0.71	This work
9.2	61.3 ± 1.2	2 ± 0.06	0.5 ± 0.13	0.96 ± 0.03	13.3 ± 1.14	5.2 ± 0.33	This work
14.4	77.5 ± 1.0	1.4 ± 0.1	0.7 ± 0.02	0.42 ± 0.07	9.6 ± 1.43	3.75 ± 0.15	This work
23	90.7 ± 0.6	1.35 ± 0.07	0.74 ± 0.02	0.35 ± 0.11	9.2 ± 1.31	3.6 ± 0.16	This work
43.1	98.4 ± 0.3	1.2 ± 0.04	0.8 ± 0.02	0.24 ± 0.05	8.4 ± 0.55	3.3 ± 0.13	This work
Base hydrolysis	90–97	5.82 ± 2.12	0.17 ± 0.04	4.82 ± 1.05	2.1 ± 0.42	—	2, 18, 19 and 95–97
Acid hydrolysis	90–95	1.96 ± 1.04	0.51 ± 0.12	0.96 ± 0.32	1.31 ± 0.27	—	2, 15, 17, 32, 41, 98
Enzymatic hydrolysis	90–98	1.68 ± 0.35	0.59 ± 0.08	0.68 ± 0.22	0.52 ± 0.07	—	21, 22 and 99–101

Comparison with acid-, base-, enzymatic-, and conventional hydrothermal hydrolysis highlights the advantages of the continuous supercritical water (SCW) process. Base-catalyzed routes show high atom economy but suffer from high PMIs and *E*-factors due to stoichiometric reagents and salt waste, while acid hydrolysis reduces material intensity but still generates significant waste and corrosion-related burdens. Enzymatic hydrolysis operates at low energy input but is typically limited by batch operation, long reaction times, and low space–time yields, which are not captured by standard green metrics. In contrast, SCW hydrolysis combines high atom economy, low PMIs, and low *E*-factors with competitive energy intensity (3.6 MJ kg^{-1} with heat recovery), while operating without added catalysts or solvents and enabling full valorization of fatty acids, partial glycerides, and glycerol.

6. Conclusions

This work demonstrates a continuous hydrothermal process for triglyceride hydrolysis using only water under sub- and supercritical conditions, enabling catalyst-free and solvent-free operation with residence times reduced to seconds. At 380 °C and 25 MPa, rapid and controllable conversion of coconut oil was achieved, allowing selective production of mono- and diglyceride-rich intermediates or near-complete hydrolysis to free fatty acids and glycerol through residence-time tuning. At an optimal residence time of 23 s, the process yielded 28.5 wt% diglycerides, 23 wt% monoglycerides, and 32 wt% free fatty acids, representing a balanced compromise between conversion rate, selectivity, and energy demand.

From a process-engineering standpoint, the continuous configuration, precise residence-time control, and absence of auxiliary chemicals constitute a clear intensification relative to conventional acid-, base-, and enzyme-catalysed hydrolysis routes. Quantitative evaluation using process mass intensity, *E*-factor, reaction mass efficiency, and energy intensity confirms high material efficiency, while integration of counter-current heat recovery reduced the external energy demand by up to 61%, demonstrating that the energetic cost of supercritical operation can be effectively mitigated.

Beyond conversion efficiency, control over reaction severity enables direct generation of functional glyceride mixtures without downstream modification. Hydrolysates enriched in mono- and diglycerides exhibited strong emulsifying performance and long-term stability, as confirmed by droplet size analysis, storage tests, and comparison with a commercial emulsifier. These results demonstrate that intermediate hydrolysis conditions provide both efficient triglyceride conversion and application-relevant functionality.

Scalability was validated on a pilot scale with stable operation at 30 kg h^{-1} and high oil concentrations without loss of selectivity. Combined with valorization of all product streams, the proposed continuous hydrothermal process provides a robust and resource-efficient platform for oleochemical production, demonstrating that ultrafast, water-only hydrolysis can simultaneously meet industrial process requirements and deliver high-performance bio-based ingredients.

Conflicts of interest

There are no conflicts to declare.

Data availability

The data supporting this article have been included as part of the supplementary information. Any other data will be available on request.

Acknowledgements

This work was supported by the Agencia Estatal de Investigación (AEI) through projects and TED2021-129837B-C42 and PID2022-140930NB-I00. This work was also supported by the Regional Government of Castilla y León (Spain) and the EU-FEDER program (CLU-2025-05). Enkeledo Menalla was funded by predoctoral contacts JCyL. Danilo Cantero was funded by the Spanish Ministry of Science, Innovation and Universities ("Beatriz Galindo" fellowship BEAGAL18/00247).

References

1 A. Gevorgyan, K. H. Hopmann and A. Bayer, *Green Chem.*, 2021, **23**, 7219–7227.
2 R. A. Sheldon, *Green Chem.*, 2023, **25**, 1704–1728.

3 H. C. Erythropel, J. B. Zimmerman, T. M. De Winter, L. Petitjean, F. Melnikov, C. H. Lam, A. W. Lounsbury, K. E. Mellor, N. Z. Janković, Q. Tu, L. N. Pincus, M. M. Falinski, W. Shi, P. Coish, D. L. Plata and P. T. Anastas, *Green Chem.*, 2018, **20**, 1929–1961.

4 A. Bardow, J. Pérez-Ramírez, S. Sala and L. Vaccaro, *Green Chem.*, 2024, **26**, 11016–11018.

5 D. Merino, A. I. Quilez-Molina, G. Perotto, A. Bassani, G. Spigno and A. Athanassiou, *Green Chem.*, 2022, **24**, 4703–4727.

6 K. V. Lira da Silva Bastos, A. B. de Souza, A. C. Tomé and F. D. M. Souza, *Plants*, 2025, **14**, 1–28.

7 D. C. Palacio Lozano, H. E. Jones, T. Ramirez Reina, R. Volpe and M. P. Barrow, *Green Chem.*, 2021, **23**, 8949–8963.

8 G. S. Luengo, F. Leonforte, A. Greaves, R. G. Rubio and E. Guzman, *Green Chem.*, 2023, **25**, 7863–7882.

9 W. Chen, R. He, R. Liu, J. Zeng, R. Liu, H. Wang, W. Guan, Z. Lv, B. Fu and W. Pu, *RSC Adv.*, 2024, **14**, 31663–31674.

10 M. Â. P. R. Cerqueira and L. M. P. Castro, *Fat mimetics for food applications*, 2023.

11 T. A. Ewing, N. Nouse, M. van Lint, J. van Haveren, J. Hugenholtz and D. S. van Es, *Green Chem.*, 2022, 6373–6405.

12 C. Spandagos, *Achieving decarbonization goals through biofuels: Policy challenges and opportunities in the European Union and the United States*, Elsevier Inc., 2023.

13 A. Mustafa, S. Faisal, I. A. Ahmed, M. Munir, E. P. Cipolatti, E. A. Manoel, C. Pastore, L. di Bitonto, D. Hanelt, F. O. Nitbani, Z. M. El-Bahy, A. Inayat, T. M. M. Abdellatief, K. Tonova, A. Bokhari and A. Abomohra, *Biotechnol. Adv.*, 2023, **69**, 108275.

14 V. Hessel, S. Mukherjee, S. Mitra, A. Goswami, N. N. Tran, F. Ferlin, L. Vaccaro, F. M. Galogahi, N. T. Nguyen and M. Escribà-Gelonch, *Green Chem.*, 2024, **26**, 9503–9528.

15 F. O. Nitbani, P. J. P. Tjitda, B. A. Nurohmah and H. E. Wogo, *J. Oleo Sci.*, 2020, **69**, 277–295.

16 L. B. Barbosa, C. M. Pacheco, I. G. da Silva, M. R. B. P. Gomez, A. S. França, G. C. Breda, M. C. Silva, P. S. de Alencar, F. A. Lima, R. A. C. Leão, R. V. Almeida and R. O. M. A. de Souza, *RSC Sustainability*, 2025, **3**, 3407–3417.

17 F. Su and Y. Guo, *Green Chem.*, 2014, **16**, 2934–2957.

18 A. Mannu, P. Almendras Flores, F. Briatico Vangosa, M. E. Di Pietro and A. Mele, *RSC Sustainability*, 2024, **3**, 300–310.

19 E. O. Ebikade, S. Sadula, Y. Gupta and D. G. Vlachos, *Green Chem.*, 2021, **23**, 2806–2833.

20 A. Baena, A. Orjuela, S. K. Rakshit and J. H. Clark, *Chem. Eng. Process.*, 2022, **175**, 108930.

21 T. A. V. Nguyen, T. D. Le, H. N. Phan and L. B. Tran, *Scientifica*, 2018, **2018**, 1–6.

22 H. Wang, H. P. Li, C. K. Lee, N. S. Mat Nanyan and G. S. Tay, *Heliyon*, 2024, **10**, e31292.

23 E. Menalla, J. G. Serna, D. Cantero and M. J. Cocero, *Chem. Eng. J.*, 2024, **493**, 152391.

24 D. A. Cantero, C. Martínez, M. D. Bermejo and M. J. Cocero, *Green Chem.*, 2015, **17**, 610–618.

25 N. Abad-Fernández, E. Pérez and M. J. Cocero, *Green Chem.*, 2019, **21**, 1351–1360.

26 E. G. Mission and M. J. Cocero, *Green Chem.*, 2022, **24**, 8393–8405.

27 V. Leontijevic, D. Cantero, S. B. Solares, A. Heredia Bayona and M. J. Cocero Alonso, *Green Chem.*, 2025, **27**, 2950–2967.

28 A. Romero, D. A. Cantero, A. Nieto-Márquez, C. Martínez, E. Alonso and M. J. Cocero, *Green Chem.*, 2016, **18**, 4051–4062.

29 M. J. Cocero, Á. Cabeza, N. Abad, T. Adamovic, L. Vaquerizo, C. M. Martínez and M. V. Pazo-Cepeda, *J. Supercrit. Fluids*, 2018, **133**, 550–565.

30 A. A. Peterson, F. Vogel, R. P. Lachance, M. Fröling, M. J. Antal and J. W. Tester, *Energy Environ. Sci.*, 2008, **1**, 32–65.

31 T. Pinnarat and P. E. Savage, *J. Supercrit. Fluids*, 2010, **53**, 53–59.

32 M. A. Peters, C. T. Alves, J. Wang and J. A. Onwudili, *ACS Omega*, 2022, **7**, 46870–46883.

33 L. K. dos Santos, R. R. Hatanaka, J. E. de Oliveira and D. L. Flumignan, *Renewable Energy*, 2019, **130**, 633–640.

34 M. A. Peters, C. Alves, J. Wang and J. A. Onwudili, *ACS Omega*, 2022, **7**, 46870–46883.

35 R. Alenezi, G. A. Leeke, R. C. D. Santos and A. R. Khan, *Chem. Eng. Res. Des.*, 2009, **87**, 867–873.

36 A. A. Hassan, H. A. Alhameedi and J. D. Smith, *Chem. Eng. Process.*, 2020, **150**, 107881.

37 F. Vedovatto, G. Ugalde, C. Bonatto, S. F. Bazoti, H. Treichel, M. A. Mazutti, G. L. Zabot and M. V. Tres, *J. Supercrit. Fluids*, 2021, **167**, 105043.

38 L. J. Visioli, C. P. Trentini, F. de Castilhos and C. da Silva, *Grasas Aceites*, 2018, **140**, 238–247.

39 P. Thakhiew, C. Kesornpun, T. Wongnate, W. Kiatkittipong and N. Weeranoppanant, *ACS Sustainable Chem. Eng.*, 2022, **10**, 14724–14734.

40 R. Alenezi, M. N. Baig, J. Wang, R. C. D. Santos and G. A. Leeke, *Energy Sources, Part A*, 2010, **32**, 460–468.

41 K. Ngaosuwan, E. Lotero, K. Suwannakarn, J. G. Goodwin and P. Praserthdam, *Ind. Eng. Chem. Res.*, 2009, **48**, 4757–4767.

42 O. Megi, T. L. Nareswari, E. Syafitri and N. Adliani, *Acta Pharm. Indones.*, 2024, **12**, 11718.

43 V. Kaushik, R. Chogale and S. Mhaskar, *J. Cosmet. Dermatol.*, 2021, **20**, 1306–1317.

44 A. Deen, R. Visvanathan, D. Wickramarachchi, N. Marikkar, S. Nammi, B. C. Jayawardana and R. Liyanage, *J. Sci. Food Agric.*, 2021, **101**, 2182–2193.

45 E. Subroto, *Food Res.*, 2020, **4**, 932–943.

46 C. C. Loi, G. T. Eyres and E. J. Birch, *J. Food Eng.*, 2019, **240**, 56–64.

47 Maxivio, *Coconut oil unrefined*, Valencia, 2025.

48 Ó. Benito-Román, E. Menalla, M. T. Sanz and D. Cantero, *Biomass Bioenergy*, 2025, **200**, 108014.

49 ISO 113581, Int. Organ. Stand., 2015, 10406–1:20, 3–6.

50 F. Rezaei, R. Jamei and R. Heidari, *Adv. Pharm. Bull.*, 2018, **8**, 115–121.

51 J. D. McCurry, *Technology*, 2008, 1–10.
52 R. Kumar and P. Singh, *J. Herb. Med.*, 2025, **49**, 100982.
53 I. G. Hwang, Y. J. Shin, S. Lee, J. Lee and S. M. Yoo, *Prev. Nutr. Food Sci.*, 2012, **17**, 286–292.
54 Y. J. Kim, I. Y. Lee, T. Kim, J. H. Lee, Y. G. Chun, B. Kim and M. H. Lee, *J. Sci. Food Agric.*, 2022, **102**, 5738–5749.
55 Y. Bao, H. Xue, Y. Yang, X. Wang, H. Yu and C. Piao, *Foods*, 2021, **10**, 2982.
56 A. Acero-Lopez, P. Schell, M. Corredig and M. Alexander, *J. Dairy Res.*, 2010, **77**, 445–451.
57 G. T. Karsli, S. Şahin and M. H. Öztop, *ACS Food Sci. Technol.*, 2022, **2**, 1832–1839.
58 Q. Fu, L. Zhou, H. Shi, R. Wang and L. Yang, *Front. Nutr.*, 202, **10**, 1125312.
59 M. Ringnér, *Nat. Biotechnol.*, 2008, **26**, 303–304.
60 P. G. C. Lucena, J. C. Carregosa, M. N. Eberlin, A. Wisniewski and J. M. Santos, *Fuel*, 2025, **384**, 133894.
61 E. Ximenes, S. Sun, D. Lachos-perez, R. M. Rodríguez-jasso, R. Sun, B. Yang and M. R. Ladisch, *Bioresour. Technol.*, 2021, **342**, 125961.
62 R. Posmanik, D. A. Cantero, A. Malkani, D. L. Sills and J. W. Tester, *J. Supercrit. Fluids*, 2017, **119**, 26–35.
63 E. Minami and S. Saka, *Fuel*, 2006, **85**, 2479–2483.
64 A. L. Milliren, J. C. Wissinger, V. Gottumukala and C. A. Schall, *Fuel*, 2013, **108**, 277–281.
65 S. Changi, T. Pinnarat and P. E. Savage, *Ind. Eng. Chem. Res.*, 2011, **50**, 12471–12478.
66 F. Valentini, F. Ferlin and L. Vaccaro, *Green Chem.*, 2025, **27**, 12166–12175.
67 F. Ferlin, F. Valentini, F. Campana and L. Vaccaro, *Green Chem.*, 2024, **26**, 6625–6633.
68 P. Krammer and H. Vogel, *J. Supercrit. Fluids*, 2000, **16**, 189–206.
69 L. Vaquerizo and M. J. Cocero, *Chem. Eng. J.*, 2019, **378**, 122199.
70 P. Khuwijitjaru, A. Pokpong, K. Klinchongkon and S. Adachi, *Int. J. Food Sci. Technol.*, 2014, **49**, 1946–1952.
71 A. M. Marina, Y. B. Che Man, S. A. H. Nazimah and I. Amin, *JAOCS, J. Am. Oil Chem. Soc.*, 2009, **86**, 301–307.
72 O. Tavakoli and H. Yoshida, *Ind. Eng. Chem. Res.*, 2006, **45**, 5675–5680.
73 Q. Shen, Z. Zhang, S. Emami, J. Chen, J. M. Leite Nobrega de Moura Bell and A. Y. Taha, *npj Sci. Food*, 2021, **5**, 1–11.
74 A. A. Khaskheli, F. N. Talpur, M. A. Ashraf, A. Cebeci, S. Jawaid and H. I. Afridi, *J. Mol. Catal. B:Enzym.*, 2015, **113**, 56–61.
75 S. N. Shah, B. K. Sharma, B. R. Moser and S. Z. Erhan, *Bioenergy Res.*, 2009, **3**, 214–223.
76 K. Gandhi, R. Sharma, R. Seth and B. Mann, *Appl. Food Res.*, 2022, **2**, 100035.
77 Ó. Benito-román, B. Blanco, M. T. Sanz and S. Beltrán, *Antioxidants*, 2020, **9**, 1–20.
78 K. M. Bromley and C. E. MacPhee, *Interface Focus*, 2017, **7**, 20160124.
79 K. Wang, K. Li, J. Tang, H. Fan, H. Wang and X. Huang, *Energy Fuels*, 2020, **34**, 16147–16157.
80 A. Pawlik, D. Kurukji, I. Norton and F. Spyropoulos, *Food Funct.*, 2016, **7**, 2712–2721.
81 D. A. Cantero, M. Dolores Bermejo and M. José Cocero, *Bioresour. Technol.*, 2013, **135**, 697–703.
82 D. A. Cantero, M. D. Bermejo and M. J. Cocero, *J. Supercrit. Fluids*, 2013, **75**, 48–57.
83 T. Adamovic, D. Tarasov, E. Demirkaya, M. Balakshin and M. J. Cocero, *J. Cleaner Prod.*, 2021, **323**, 129110.
84 S. Chumsantea, K. Aryusuk, S. Lilitchan, N. Jeyashoke and K. Krisnangkura, *JAOCS, J. Am. Oil Chem. Soc.*, 2012, **89**, 1913–1919.
85 F. Seifollahi, M. H. Eikani and N. Khandan, *J. Cleaner Prod.*, 2024, **454**, 142304.
86 K. Werth, P. Kaupenjohann and M. Skiborowski, *Sep. Purif. Technol.*, 2017, **182**, 185–196.
87 M. Fortunatti-Montoya, F. A. Sánchez, P. E. Hegel and S. Pereda, *J. Supercrit. Fluids*, 2019, **153**, 2–11.
88 S. Mhadmhan, B. Yoosuk, B. Chareonteraboon, P. Janetaisong, P. Pitakjakpipop, S. Henpraserttae and P. Udomsap, *Sep. Purif. Technol.*, 2023, **310**, 123211.
89 A. Khoramnia, A. Ebrahimpour, R. Ghanbari, Z. Ajdari and O. M. Lai, *Biomed. Res. Int.*, 2013, **2013**, 7–9.
90 E. Prudnikov, H. Abu Hamad, I. Polishchuk, A. Katsman, E. Segal and B. Pokroy, *ACS Appl. Bio Mater.*, 2025, **8**, 5970–5983.
91 D. Y. C. Leung, X. Wu and M. K. H. Leung, *Appl. Energy*, 2010, **87**, 1083–1095.
92 S. S. Yazdani and R. Gonzalez, *Curr. Opin. Biotechnol.*, 2007, **18**, 213–219.
93 Z. Hubálek, *Cryobiology*, 2003, **46**, 205–229.
94 A. Mortensen, F. Aguilar, R. Crebelli, A. Di Domenico, B. Dusemund, M. J. Frutos, P. Galtier, D. Gott, U. Gundert-Remy, J.-C. Leblanc, O. Lindtner, P. Moldeus, P. Mosesso, D. Parent-Massin, A. Oskarsson, I. Stankovic, I. Waalkens-Berendsen, R. A. Woutersen, M. Wright, M. Younes, P. Boon, D. Chrysafidis, R. Gürtler, P. Tobback, A. M. Rincon, A. Tard and C. Lambré, *EFSA J*, 2017, **15**, e04720.
95 J. P. Pasanen, A. Malm and R. Piilola, A process for producing free fatty acids, *WO Pat.*, WO2019122519A1, 2019.
96 W. R. Sutterlin, R. A. Long, C. O. Blanchard and J. Brown, Methods for making free fatty acids from soaps using thermal hydrolysis followed by acidification, *US Pat.*, US9745541B1, 2017.
97 Chemistry Education Research and Practice, R. Soc. Chem, chem 1100 Appendix 2, 2017, 2–5https://www.rsc.org/suppdata/c7/rp/c7rp00133a/c7rp00133a2.pdf.
98 N. A. Serri, A. H. Kamarudin and S. N. Abdul Rahaman, *J. Phys. Sci.*, 2008, **19**, 79–88.
99 E. Faillace, V. Brunini-Bronzini de Caraffa, M. Mariani, L. Berti, J. Maury and S. Vincenti, *Int. J. Mol. Sci.*, 2023, **24**, 12274.
100 B. C. Páez, A. R. Medina, F. C. Rubio, P. G. Moreno and E. M. Grima, *Enzyme Microb. Technol.*, 2003, **33**, 845–853.
101 A. Baena, A. Orjuela, S. K. Rakshit and J. H. Clark, *Chem. Eng. Process.*, 2022, **175**, 108930.